3-24-2016

Comparison of Methods for Radio Position of Non-Emitting Dismounts

Collin J. Seanor

COMPARISON OF METHODS FOR RADIO POSITION OF NON-EMITTING DISMOUNTS

THESIS

Collin J. Seanor, Captain, USAF

AFIT-ENG-MS-16-M-044

DEPARTMENT OF THE AIR FORCE
AIR UNIVERSITY

AIR FORCE INSTITUTE OF TECHNOLOGY

Wright-Patterson Air Force Base, Ohio

AFIT-ENG-MS-16-M-044

COMPARISON OF METHODS FOR RADIO POSITION OF NON-EMITTING DISMOUNTS

THESIS

Presented to the Faculty

Department of Electrical and Computer Engineering

Graduate School of Engineering and Management

Air Force Institute of Technology

Air University

Air Education and Training Command

in Partial Fulfillment of the Requirements for the

Degree of Master of Science in Electrical Engineering

Collin J. Seanor, B.S.

Captain, USAF

March 2016

AFIT-ENG-MS-16-M-044

COMPARISON OF METHODS FOR RADIO POSITION OF NON-EMITTING DISMOUNTS

THESIS

Collin J. Seanor, B.S.
Captain, USAF

Committee Membership:

Dr. Richard K. Martin
Chair

Dr. Peter J. Collins
Member

Dr. Michael A. Temple
Member

Abstract

Radio Tomographic Imaging (RTI) is a form of Device Free Passive Localization (DFPL) that utilizes the Received Signal Strength (RSS) values from a collection of wireless transceivers to produce an image in order to localize a subject within a Wireless Sensor Network (WSN).

Radio Mapping is another form of DFPL that can utilize the same RSS values from a WSN to localize a subject by comparing recent values to a set of calibration data.

RTI and Radio Mapping have never been directly compared to one another as a means of localization within a WSN. The goal of this research is to compare using TelosB mote devices these approaches in a side-by-side manner. A real world WSN was constructed and both RTI and Radio Mapping methodologies were applied to identical data sets with the results compared and discussed.

Initial results show that both methodologies have inherent advantages and disadvantages respective to one another; Radio Mapping performs significantly better in WSNs with a low number of transceivers being 100% accurate within the bounds of this experimentation, while RTI has significantly more simple calibration procedures.

Acknowledgements

First and foremost I would like to thank my wife who has supported me though this endeavor and throughout the great adventure that is our life. I am nothing without you.

Additionally I would like to thank my advisor for enabling me; and my fellow students for assisting me through this degree program. Finally I would like to thank the Air Force and AFIT for giving me the opportunity to further my education.

Collin J. Seanor

Table of Contents

Page

Page

List of Figures

COMPARISON OF METHODS FOR RADIO POSITION OF NON-EMITTING DISMOUNTS

I. Introduction

This chapter gives a brief introduction to WSNs and the fundamentals of RTI and Radio Mapping. It provides an overview of the background of RTI and Radio Mapping, problem statement for this thesis, goal of the research conducted and the structure for the remainder of the document.

1.1 Background

Increases in modern technology have led to the advent of DFPL as a legitimate means to locate a target inside of a WSN. A WSN is a series of sensors arranged in a specific and known geometry, each acting as a radio transceiver, both listening to and sending out signals in turn. The information gathered from these sensors is often used to localize a subject within the WSN. [1]

Until recently, localization had been primarily conducted with the subject wearing an active device, with data gathered from sensors used to triangulate the subjects position, or in the case of GPS, the subject's device gathers data and triangulates position of the user. DFPL does not require the subject to be wearing a device. This is based on the concept that the subject's physical body attenuates Radio Frequency (RF) signals that propagate through it, and this phenomenon can be used in a WSN for subject localization. This concept has a multitude of applications, in any environment in which a subject is unwilling or unable to wear or use a personal device, or the utilization of such device is impractical [2].

Radio Tomographic Imaging.

A RTI system generally performs localization by gathering data from a WSN utilizing RF transceivers. The transceivers within the system are constantly establishing links with each other. The primary information recorded from these sequential links is the RSS. Because the human body attenuates Radio Waves, a RF link between transceivers that linearly intersects with the subject will have a lower RSS. The area within the WSN is generally split into a grid of pixels, with a weight matrix generated to determine what pixels are affected by what links, and how much each pixel affected by that link is impacted by the value of that link. The weight matrix and the RSS values are then utilized to calculate a gray-scale image of attenuation changes in the area covered by the WSN [1].

A significant advantage to this approach is, due to RF's ability to pass through the walls of most modern structures; a RTI based WSN can map and detect movement in a building through walls. Additionally if a WSN were to be calibrated while empty, it can accurately predict the location of human beings even if they remain still. Possible real world applications of RTI systems vary and include elderly care, security systems, disaster response, and special forces utility [3].

Radio Mapping.

Like RTI Radio Mapping is a form of DFPL utilizing a WSN. However, instead of utilizing attenuation values to generate an image, a Radio Mapping system compares attenuation values to a pre-calibrated set of values to determine the location of the subject.

Advantages to this approach are its computational simplicity, and specific output. A Radio Mapping system outputs a specific, determined location region for the subject. The uncertainty within this output is determined by the number of calibration

points within the WSN relative to the size of the WSN.

1.2 Problem Statement

Despite the significant amount of research done and great potential of RTI systems, there remain significant gaps in current research and capabilities. Radio Mapping has significantly less research yet there are readily apparent problems with it's methodology as well.

Frame Rate.

An increase in the number of transceivers will lead to an increase in data. It also increases the time for the system to capture one full frame of data; with an increased capture time, it becomes much more difficult to determine the precise location of a moving target at any specific time [4]. This issue is perverse in both systems, therefore the system that can accurately produce localization results with a smaller amount of data will have a higher frame-rate.

Multi-path.

While the most powerful signal linking two transceivers will generally be the Line of Sight (LoS) signal, a significant amount of multi-path often will interfere with a physical obstruction's ability to attenuate the measured RSS. Additionally a physical interference within a particularly strong multi-path can lead to a false positive of attenuation between links. This can lead to decreased accuracy in an RTI system. The effects of multi-path on a Radio Mapping system are less so. The calibration data set records the RSS values with a subject at a specific set of locations; therefore any multi-path signals are "factored in" to the calibration set and are removed as an error source.

Computational Complexity.

An increase in the number of transceivers leads to an exponential increase in the computational complexity of an RTI system. This increase can demand large amounts of memory, and take an ever increasing amount of computational power to generate an image. Ultimately given a network of equal size, Radio Mapping will be less computationally complex than an identical WSN in an RTI system. [4]

Calibration time.

Unlike computational complexity, calibration time is a advantage that RTI has over Radio Mapping. Chapter II will discuss in detail the amount of calibration required for RTI systems, however the amount of calibration required by a Radio Mapping system grows exponentially with desired precision.

1.3 Research Goal

The goal of this research is to utilize Radio Mapping with WSNs in comparison to typical RTI systems under identical conditions. This will be done in order to ascertain the impact of such techniques on the accuracy and robustness of a localization system. Radio Mapping has the potential to eliminate the multi-path issues that currently exist in specific RTI configurations, additionally requiring a decreased amount of sensors to achieve an accurate localization; resulting in increased frame rate and decreased computational complexity. Ultimately a side by side comparison of RTI and Radio Mapping systems will be delivered in the form of superimposed images.

1.4 Approach

This thesis includes the use of physical experiments to pursue the research goals. RTI and radio mapping experiments were done attempting to locate a subject within

an operational WSN. The conditions and subject involved in these experiments were kept uniform between all of the gathered data sets.

1.5 Thesis Structure

The remainder of this thesis is broken down into four chapters, Chapter II provides an in depth review of the current research, literature, background science, and modeling methods involved in WSNs, RTI systems and Radio Mapping. Chapter III outlines the techniques and methodology used in conducting this research. Then chapter IV discloses all relevant data and analytical results of the experiments conducted. Finally, Chapter V draws conclusions from the results disclosed in Chapter IV as well as outlines possible future research drives.

II. Related Work

This chapter explores the background and theory of both RTI and Radio Mapping systems. First key terms are defined, followed with an in depth analysis of weight matrices, regularization, and measurement methodologies. Finally, this chapter will identify a current gap in research.

2.1 Radio Tomographic Imaging Overview

RTI is a novel method of DFPL that utilizes RSS values within a WSN. An in depth look at the RTI model will be discussed in the next section after the supporting terminology, such as DFPL and WSN, has been adequately defined and discussed [5], [2].

Device Free Passive Localization.

DFPL is a method of localization that does not require any signal emission from the target being localized, nor does it require any device, passive or otherwise, to be carried or attached to the target [1], [6].

This represents a very unobtrusive and discrete method of tracking individuals and has many obvious applications in both civilian and government usage; such as patient or elderly monitoring, roadside surveillance, security, special forces room clearance and entry [7].

Wireless Sensor Network.

A WSN is a group of sensors networked together and physically positioned in a chosen geometry around an Area of Interest (AoI). Each node in the network transmits sequentially, with every other node listening; the RSS value from each

transmission, or unique link, is recorded and becomes the raw data used in the RTI process, ultimately producing an image [8].

The number of unique links in a WSN is tied directly to the number of sensors in the WSN. The number of unique links, and therein the amount of useful data gathered by a WSN, can be modeled as [9]

$$U = (N^2 - N)/2, \tag{1}$$

with N being the number of WSN sensors and U being the number of unique links/-data values generated during one "frame."

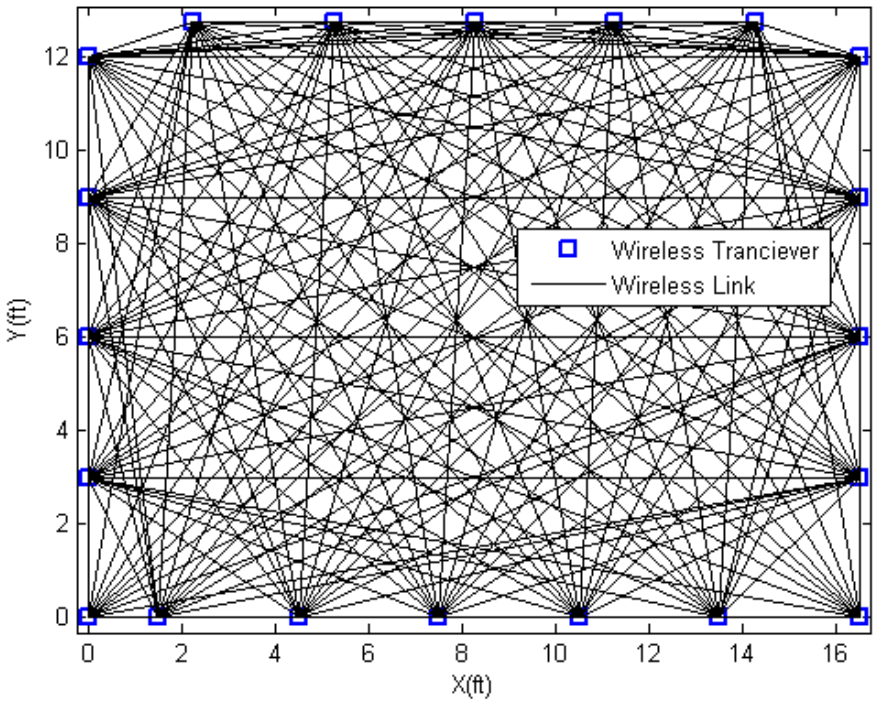

Figure 1. Example of all the links present in a 20 mote WSN

With a larger number of sensors, an exponentially larger amount of data is produced. While this can can lead to an ultimately more accurate image, each sensor must fire sequentially. Therefore increasing the number of sensors leads to a decrease

in frame-rate, as each sensor must fire before the frame is "complete," which leads to difficulty accurately tacking moving targets. Additionally, the amount of data can become overwhelming for modern computational systems [9].

Received Signal Strength.

The value measured in the unique links mentioned above is the RSS of each transmission. This forms the entirety of the data necessary to produce an image.

The transceivers within the WSN transmit at frequencies that follow line of sight propagation, given negligible noise, multi-path and interference. A decrease in the RSS at a specific link indicates a new obstruction between those two links. This provides the premise for generating an image from calibrated RSS data [7].

2.2 RSS RTI Model

As discussed earlier, RTI utilizes the received signal strength of the transceivers in the WSN to generate an attenuation image of the area within the WSN.

The RTI system model was first pioneered by Wilson and Patwari [9]. In their work, a number N sensors are configured in a WSN around an area of interest.

As addressed earlier, each sensor "links" with every other sensor. The RSS measured in these links provides the totality of information used in generating an RTI image. There are various methods of RSS image production discussed later, however ultimately a vector of every RSS value $\boldsymbol{y}$ is utilized in the RTI system model.

The area within the WSN is split into a group of pixels, the size of which can be variable. The implications of pixel size choice can have significant impact on the accuracy and resolution of the image produced as discussed in [10]. In short, the larger the pixel the more accurate your image will be as more links fall within each pixel, giving more information and therefore a more accurate image. As pixel size

decreases the resolution of the image increases; but with each pixel's value being calculated using less and less information, the overall accuracy of each pixel will decrease. Ultimately, with the pixel size chosen, a vector $\boldsymbol{x}$ of all the pixels within a specific WSN is utilized.

A weight matrix, $\boldsymbol{W}$, is compiled to determine the effect that each link will have on each pixel. The specifics of this compilation, as well as the different types of weight matrix models, will be discussed in a later section.

For the purposes of the RTI model, all noise power is grouped together in a vector for each specific link, $\boldsymbol{n}$. Noise is further discussed in the next section.

Ultimately, these four variables are used for the surprisingly simple RTI model written in matrix form as [9]

$$\boldsymbol{y} = \boldsymbol{W}\boldsymbol{x} + \boldsymbol{n}. \tag{2}$$

The method of extracting an accurate estimate for pixel values $\boldsymbol{x}$, in the presence of an ill-conditioned $\boldsymbol{W}$, otherwise known as regularization, is discussed in a later section.

2.3 Noise Model

Significant experimentation has been done in an attempt to model the different types of noise encountered in an RTI system [1], [10], [11]. Nannuru states in [11] that Additive White Gaussian Noise (AWGN) is a sufficient model for a RTI system. AWGN is a relatively common distribution utilized in noise modeling, and is easy to simulate and account for, given its zero mean. Most noise values whether environmental, transmitter, receiver, or fading based are grouped into a single AWGN term labeled $\boldsymbol{n}$ [12].

In [10] Martin determined that an AWGN distribution model with a standard

deviation of 6dB was appropriate for a WSN utilizing TelosB motes, which are the same transceivers used for experimentation in this thesis, and therefore an estimated AWGN of 6dB will be used [9], [12].

Multi-path.

A considerably difficult error source to model within an RTI system is that of multi-path. While all other noise parameters can be assumed Gaussian in distribution, multi-path can vary wildly between network setups, depending on the environment and specific frequencies being used by the transceivers. This document's exploration into radio-mapping may prove as a useful tool to combat this nuisance parameter [13].

2.4 Regularization Methodology

Given the RTI system model $\boldsymbol{y} = \boldsymbol{W}\boldsymbol{x} + \boldsymbol{n}$, the pixel value $\boldsymbol{x}$ must be extracted in order to produce an estimated image of the area within the WSN. Multiple regularization systems exist in an effort to minimize the noise generated by this process [9], [14].

Initially, a least-squares solution appears to be the obvious choice taking

$$\hat{\boldsymbol{x}} = \arg\min_{x} \|\boldsymbol{W}\boldsymbol{x} - \boldsymbol{y}\|^2 \tag{3}$$

and solving it to get

$$\hat{\boldsymbol{x}} = (\boldsymbol{W}^T\boldsymbol{W})^{-1}\boldsymbol{W}^T\boldsymbol{y}. \tag{4}$$

An issue arises, however, because the matrix $(\boldsymbol{W}^T\boldsymbol{W})$ is generally not invertable, or considered not full rank, therefore making the estimate of $\boldsymbol{x}$ to be considered an

ill-posed inverse problem [14].

Linear Back Projection.

The simplest technique to solve this ill-posed inverse problem is that of Linear Back Projection as discussed in [14] and [15]. This solution simply drops the un-invertible matrix ($\boldsymbol{W}^T\boldsymbol{W}$) from the least squared solution giving

$$\hat{\boldsymbol{x}} = \boldsymbol{W}^T\boldsymbol{y}. \tag{5}$$

However, the values of the weight matrix $\boldsymbol{W}$ are generally smaller than the values of the noise vector $\boldsymbol{n}$ and this method of Linear Back Projection amplifies those error values, and generally produces images of poor accuracy [15].

Tikhonov Regularization.

Tikhonov regularization is the most commonly used form of regularization for any ill-posed inverse problem regardless of field, and is also the most commonly used form within the specific practice of RTI. The reason for its popularity is that ultimately the solution for the regularization is only a simple linear transformation of the recorded RSS values [14]

$$\hat{\boldsymbol{x}} = \Pi\boldsymbol{y}. \tag{6}$$

In order to determine our linear transformation, Tikhonov regularization begins by adding an energy term to the initial least square equation, which creates the objective function [9]

$$f(x) = \frac{1}{2}||\boldsymbol{W}\boldsymbol{x} - \boldsymbol{y}||^2 + \alpha||\boldsymbol{Q}\boldsymbol{x}||^2. \tag{7}$$

The matrix $\boldsymbol{Q}$ is the Tikhonov matrix. The parameter α is considered the regularization parameter; this is a value that can be changed to affect the noise and overall smoothing of the image. As the value of α is increased, the image is smoothed, with both noise and true values being lost. A decrease in α will increase the amount of noise still present in the image, but will truncate the true values within said image less. The specific value of α is usually manipulated by the user of an RTI system to their specific needs and desires [9].

In [1] the Tikhonov matrix is extrapolated to be the combination of a matrix $\boldsymbol{D}_{\mathrm{x}}$, or the "difference operator in the horizontal direction" and $\boldsymbol{D}_{\mathrm{y}}$, "the difference operator in the vertical direction" the resulting objective cost function is [14]

$$f(x) = \frac{1}{2}||\boldsymbol{W}\boldsymbol{x} - \boldsymbol{y}||^2 + \alpha(||\boldsymbol{D}_{\mathrm{x}}\boldsymbol{x}||^2 + ||\boldsymbol{D}_{\mathrm{y}}\boldsymbol{x}||^2). \tag{8}$$

The derivative of this equation is then taken with the result set equal to zero, which provides the solution

$$\hat{\boldsymbol{x}} = (\boldsymbol{W}^T\boldsymbol{W} + \alpha(\boldsymbol{D}_{\mathrm{x}}^T\boldsymbol{D}_{\mathrm{x}} + \boldsymbol{D}_{\mathrm{y}}^T\boldsymbol{D}_{\mathrm{y}}))^{-1}\boldsymbol{W}^T\boldsymbol{y}. \tag{9}$$

This solution leads us to our final linear operator as spoken to earlier in this section

$$\boldsymbol{\Pi} = (\boldsymbol{W}^T\boldsymbol{W} + \alpha(\boldsymbol{D}_{\mathrm{x}}^T\boldsymbol{D}_{\mathrm{x}} + \boldsymbol{D}_{\mathrm{y}}^T\boldsymbol{D}_{\mathrm{y}}))^{-1}\boldsymbol{W}^T. \tag{10}$$

This operator is the function of three main variables; the weight matrix, whose calculation will be spoken to in the next section; the pixel size and the regularization parameter, both chosen by the user.

2.5 Weight Matrix Modeling

The values within the weight matrix $\boldsymbol{W}$ are responsible for determining how much each RSS value $\boldsymbol{y}$ has on each respective pixel. The models for determining the specific values within this weight matrix vary from complex and accurate to fast and simple. The specific model used is chosen by the user for their specific needs.

All weight matrix models split the matrix into two unique parts via the equation [16]

$$\boldsymbol{W} = \boldsymbol{\Omega} \odot \boldsymbol{S}. \tag{11}$$

In this equation, $\boldsymbol{S}$ is a binary selection matrix, a matrix full of ones and zeros, determining if each specific pixel is at all affected by the specific link. The $\boldsymbol{\Omega}$ matrix is a set of real values, specifically, a scalar of how much each pixel is effected by the designated link. Finally $\odot$ is Hadamard multiplication, or element-wise multiplication, making both $\boldsymbol{S}$ and $\boldsymbol{\Omega}$ the same dimensions as $\boldsymbol{W}$ [14].

There are three primary models for deriving the values of $\boldsymbol{S}$ and $\boldsymbol{\Omega}$. They are the Line Model, the NeSh Model, and the Line-NeSh Model [16], [17], [18].

Line Model.

Line model has been used in a number of of RTI systems. It's key advantage is that is relatively simple to implement and computationally efficient [16]. It can, however, "miss" the target in certain instances making other models generally more popular [19] [17].

The line model is only concerned with the pixels that a strait line drawn between the two transceivers in question directly passes through. Therefore, the selection matrix is $\boldsymbol{S} = 1$ for any pixel p that has a link l passing though it and $\boldsymbol{S} = 0$ for all

other. Written mathematically [19],

$$\boldsymbol{S} = \begin{cases} 1, & \text{if line between trancievers traverses pixel} \\ 0, & \text{else} \end{cases}. \tag{12}$$

See Figure 2 for a graphical representation of this equation for the selected pixels given a specific link.

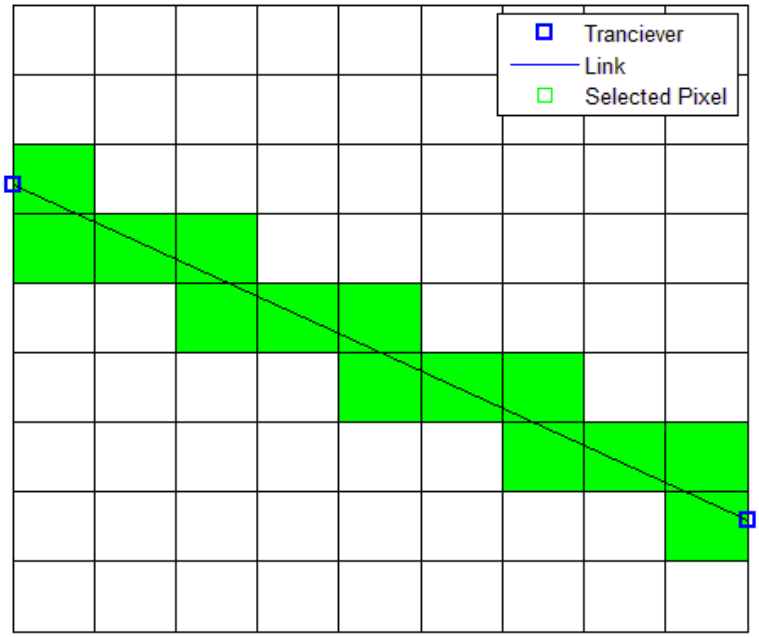

Figure 2. Graphic of selected pixels in the Line Model for weight matrix derivation

The amount that these selected values are scaled by the $\boldsymbol{\Omega}$ matrix is directly related to $L_{l,p}$, or how much of the link passes through said pixel, this gives heavier weight to pixels that the link passes directly through and gives lower weight to pixels that the the link merely "skims". This model is mathematically written as [19]

$$\boldsymbol{\Omega} = SL_{l,p}. \tag{13}$$

This equation, when combined with our equation for $\boldsymbol{S}$, gives our ultimate line model weight matrix equation of [19]

$$\boldsymbol{W}_{l,p} = SL_{l,p} \begin{cases} 1, & \text{if line between trancievers traverses pixel} \\ 0, & \text{else} \end{cases}. \tag{14}$$

NeSh Model.

The NeSh Model, or Network Shadowing Normalized Ellipse Model, is the most commonly used weight matrix model in RTI systems [20], [21], [22]. The key advantage to the NeSh model is overall accuracy, this accuracy stems from the heavier weight placed on shorter links. The selection matrix also varies from that of the line model. An ellipse with a focus at each transceiver is used to determine affected pixels. Pixels that lie within the ellipse are selected and those outside ignored. This process can be mathematically written as [9], [20],

$$\boldsymbol{S}_{l,p} = \begin{cases} 1, & \text{if } d_{l,pcenter}(1) + d_{l,pcenter}(2) < d_l + \lambda \\ 0, & \text{else} \end{cases}, \tag{15}$$

where $d_{l,pcenter}$ is the distance between the transceiver and the center of the pixel in question. Refer to Figure 3 for a graphical representation of this process.

The λ value determines the width of the ellipse used in the selection process. A wider ellipse leads to the inclusion of more pixels, which can smooth out the image but leads to a loss in information. A narrow ellipse can lead to increased noise in the image [20].

The $\boldsymbol{\Omega}$ matrix is the same for each pixel selected in a link; however, it is inversely proportional to the square root of the distance of that link. In equation form,

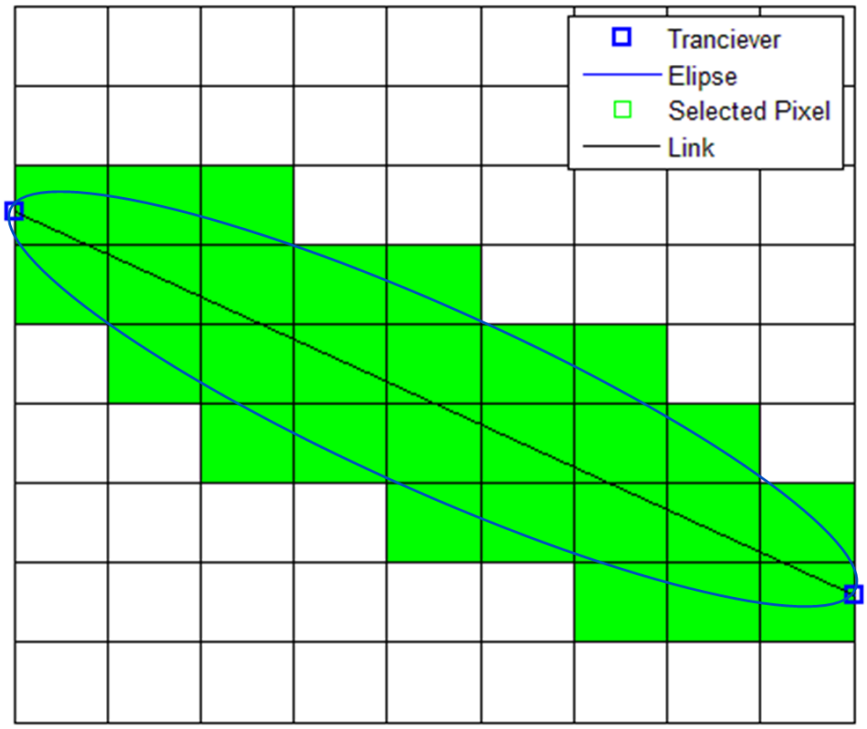

Figure 3. Graphic of selected pixels in the NeSh Model for weight matrix derivation

$$\boldsymbol{\Omega}_{l,p} = \frac{1}{\sqrt{d_l}}. \tag{16}$$

These two equations combine via the Hadamard multiplication operator to form the final NeSh Model weight matrix equation of

$$\boldsymbol{W}_{l,p} = \frac{1}{\sqrt{d_l}} \begin{cases} 1, & \text{if } d_{l,pcenter}(1) + d_{l,pcenter}(2) < d_l + \lambda \\ 0, & \text{else} \end{cases}. \tag{17}$$

NeSh-Line Model.

The NeSh-Line model is a combination of both the NeSh Model, in that the scalar operator matrix $\boldsymbol{\Omega}$ is inversely proportional to the distance between the links; and the line model, because it only selects pixels that align between the two transceivers

directly intersects. Additionally, the amount of line in each pixel also scales the value of its respective element in $\mathbf{\Omega}$. This combination mathematically represents itself as [18]

$$\boldsymbol{W} = \frac{SL_{l,p}}{\sqrt{d}} \begin{cases} 1, & \text{if line between tranceivers traverses pixel} \\ 0, & \text{else} \end{cases} . \tag{18}$$

2.6 Measuring Methods

The specific method in which RSS is measured and utilized has a significant impact on the overall image production. Shadowing loss based RSS for an RTI system requires pre-calibration but is capable of showing objects that are still within the WSN [7]. Variance based RSS systems do not require calibration to show moving objects within the WSN [23]. Finally, Kernel distance based RTI systems offer a hybrid of the two methodologies, utilizing histograms. An in-depth analysis of these methods and their specific advantages and disadvantages is discussed throughout the remainder of this section.

Shadowing Loss.

Shadowing loss based RTI systems are some of the most common and straightforward RTI systems. This method of measurement involves comparing the RSS of the WSN at the time in question to the RSS at a prior, calibration time. This baseline calibration is done by gathering the RSS values of the system for a period of time prior to system implementation without any of the subjects present within the WSN [23].

When the RSS of the system is measured again while the system is active, only the change in RSS relative to the calibration period is utilized in the calculations

described above. By comparing data between two points in time, all static variables are canceled out. Shadowing loss from stationary objects in the WSN, including walls, are ignored in the final calculation, even certain noise elements, such as background environmental noise and transceiver noise are eliminated unless those noise values have changed from the time of calibration. The result is that the only change in RSS attenuation should be a result of the presence of a new object or individual. The resulting gray-scale image produced will show the location of any objects or individuals new to the environment since the time of calibration [9], [24].

A key advantage of the shadowing loss based approach to RTI is the ability to see stationary objects, being individuals or new objects, additionally with a single per-calibration value, the computational needs are relatively simple. A disadvantage to shadowing loss approach is that the need for prior calibration limits the implementation of a system utilizing this form of RTI to pre-fabricated systems, such as possibly a security system. Additionally any stationary objects that are inadvertently moved within the WSN will show up as foreign objects triggering false positives and cluttering any produced image [24].

Variance.

A variance based approach to an RTI system addresses the weaknesses of the shadowing loss approach by measuring the the variance of RSS values over a period of time opposed to comparing the actual RSS values to a calibrated time. This approach is vary diametric in its advantages and disadvantages when compared to shadowing based RSS. By only utilizing the variance in RSS values over the current period of time, the need for a system calibration is eliminated. This adds a robustness to any real-world system in allowing first responders to set up a system ad-hoc around an area or building of interest. Additionally stationary variables such as background noise

and transceiver noise are still eliminated from the overall equation. The disadvantages are that if the target remains still it will not be properly localized by the system, and if the target moves slowly enough they will not affect the variance of the overall RSS enough within the period in question. Finally, if the time period of variance calculation is too long any rapid movements may not be realized by a variance based system in time to be properly utilized by the operators [23], [25].

Kernel Distance.

Kernel distance is a measurement model utilizing two separate histograms to act as a hybrid between both shadowing based and variance based RSS systems. Kernel distance based RTI takes both a long histogram and a short histogram of the RSS values within the WSN. The duration of these histograms is adjusted by the user to fit their specific needs. The kernel distance between these two is calculated as [21], [26],

$$\boldsymbol{\Delta}(\boldsymbol{h}_{l,s}, \boldsymbol{h}_{l,l}) = \boldsymbol{h}_{l,s}^{\boldsymbol{T}} \boldsymbol{K} \boldsymbol{h}_{l,s} + \boldsymbol{h}_{l,l}^{\boldsymbol{T}} \boldsymbol{K} \boldsymbol{h}_{l,l} - \boldsymbol{2} \boldsymbol{h}_{l,s}^{\boldsymbol{T}} \boldsymbol{K} \boldsymbol{h}_{l,l}, \tag{19}$$

with the variables $h_{l,s}$ $h_{l,l}$ representing a short term histogram and long term histogram respectively, and K is the kernel matrix. The kernel distance for each link then becomes the $\boldsymbol{y}$ vector in our calculations and image production. Ultimately [26] determined that kernel distance was a viable hybrid of the two previously mentioned designs, able to correctly locate targets both still and moving. The only relative weaknesses of kernel based RTI is that it is computationally intensive and demands significant amount of memory. Additionally, any object remaining still longer than the length of the long term histogram will "drop off" of the image [21].

2.7 Image Production

An RTI system, having chosen from the various methods of measurement, weight-matrix modeling, and regularization methods described in detail above, will ultimately produce a gray-scale image of the area within the WSN. This image is the collection of all pixel attenuation values from every link. This summation will result in a spike at the pixels in which any obstruction is located, giving an accurate location for any targets within the WSN [7].

2.8 Radio Mapping

Radio Mapping was first introduced in [27] where instead of a TelosB based RTI network, a subject's effect on the signals from a wireless network were mapped, and that map was used to then determine a subjects location at any given time.

Generating a Radio Map.

Generating a Radio Map requires extensive pre-calibration of the WSN and post processing systems. Data is captured with localization subjects at resolution locations, and stored for utilization during post processing.

As the number of subjects assumed to possibly be within the WSN increases linearly, the number of calibration data sets increases exponentially. The total number of calibration data sets required can be modeled mathematically as,

$$C = \sum_{i=0}^{n} p^i, \tag{20}$$

with n being the number of people the calibrated map can sustain, and p being the number of decision regions or "pixels" within the WSN. This equation takes into account that the subjects could possibly be within the same decision region of the

WSN. This event would result in different RSS values and must be accounted for.

This is only one approach to calibration of a Radio Map. Other calibration procedures proposed go with a more binary, "is something there" approach, calibrating a yes/no value for each pixel and then determining the locations of subjects within the WSN. While this approach streamlines the calibration process, the accuracy of this system, specifically with use of LoS transceivers, has yet to be verified. [28]

Using a Radio Map.

To utilize a Radio Map captured data from the WSN is compared to previously calibrated data. Generally a least squares approach is used, to determine where the localization subject(s) are; the calibration data that is closest to the captured data is considered truth, and the subject(s) location(s) outputted.

Advantages to Radio Mapping.

Radio Mapping has all of the major advantages that any DFPL system has in addition to a few others. A key and unique advantage of Radio Mapping is revealed by the brevity of the previous section; utilizing a Radio Map as a means of DFPL is computationally simple to execute and displaying localization data in real time is not taxing for virtually any modern computational device. Additionally, Radio Mapping delivers a discrete output for the subject's determined location, eliminating the need for any further post processing by either user or programming. Finally, a Radio Map can have significant noise resiliency, as noise elements are contained within the calibration data set this includes multi-path signals, as an attenuation, or lack there of, is accounted for in the calibration data [29].

Shortcomings of Radio Map Methodology.

The most prevalent drawback of a Radio Map DFPL system is that there is an extensive calibration time, which grows exponentially as the number of subjects N increases. If only one subject is assumed within the WSN, then calibration data must be taken for each desired localization region or effective pixel. There is a linear increase in the amount of calibration data for a linear increase in the number of pixels. [30]

Attempts to alleviate the significant amount of calibration required for a robust Radio Mapping system by generating a "learning" methodology of mapping have been made in [31]; but the issue of calibration is still a problem for any Radio Mapping system.

This Radio Mapping approach has not been adequately compared to that of typical RTI systems, and is thus the approach of this thesis, and will be discussed in detail in the following chapter.

2.9 Chapter Summary

This chapter explained in depth the various approaches and models by which RTI localization and DFPL is accomplished utilizing WSNs. DFPL, WSN, and RTI were all defined in detail within this section as well as in depth analysis of, weight matrix modeling, regularization methodology and the various approaches to RSS measurement. Additionally an in depth explanation of Radio Mapping as a form of DFPL was given. Finally a key gap in current research, Radio Mapping in comparison to typical RTI was identified. The methodology of how this thesis will fill this identified research gap is discussed in detail in the following chapter.

III. Methodology

This chapter will describe in detail the methodology and procedures utilized in the experimentation of this thesis. It begins by outlining the goals of experimentation, describes the two different system models chosen for RTI and Radio Mapping respectively, and describes key assumptions made in experimentation. The equipment and software are described in detail, as well as the physical setup of the WSN utilized in this experimentation. Finally the experiment design and procedures used are outlined, and the key metrics are identified.

3.1 Experiment Goals

The primary goal of this experimentation is to execute a side by side comparison of an RTI system and a Radio Mapping system in a real world WSN utilizing TelosB transceiver motes. Both systems will be applied to the same data sets with the resulting localization images compared. In total 837, unique data sets were gathered in an attempt to fully diagnose the comparative advantages and disadvantages of each system.

3.2 System Model

This experiment compares RTI based DFPL and Radio Map based DFPL. Two unique system models are used.

RTI Measurement Model.

For the RTI potion of experimentation, the shadowing loss model was chosen because, with its required pre-calibration period, it is the most similar to Radio Mapping of the various measuring methodologies. Variance based RTI could never

be replaced by Radio Mapping because the key advantage of variance based RTI is it doesn't require pre-calibration.

Weight Matrix Model.

The weight matrix model selected was the line model, the line model was chosen for it's simplicity and the resultant lower computational complexity. As discussed in the previous chapter, Radio Mapping has a relatively simple computation. In order to make a side by side comparison of RTI and Radio Mapping more fair, a deliberate effort was made to select an overall RTI model as similar to Radio Mapping as possible.

Chosen Regularization Methodology.

As described in the previous chapter, Tikhonov's first order regularization is the most commonly utilized form of regularization in RTI literature today. Therefore, it was chosen as the regularization methodology for the RTI system in this experimentation.

Radio Map Model.

As spoken to in the previous chapter Radio Mapping requires the production and calibration of an extensive Radio Map prior to operation. For this experimentation data was collected at 12 unique points within the WSN. See Figure 4 for a diagram of the collection points within the WSN. For calibration collection purposes a foam block was used in place of a person; see Figure 10 for an image of the foam block. This block was chosen for its relative equivalency in size to any possible human subject, but also because is was significant easier to calibrate with, as it is naturally motionless. 60+ frames of data were taken of the block at each one of the location points, summing to 837 frames in total. The number of these frames utilized in the

calibration of the Radio Map was manually varied to test the robustness of Radio Mapping as a DFPL system. The calibration map was formed by finding the mean value for each link across the total number of calibration frames for each calibrated location. The end result is 12 frames of data, one for each calibrated location. These frames form our expected value, in a basic least squares estimator,

$$\hat{\boldsymbol{x}} = \arg\min_{x} \|\boldsymbol{x}_{cal} - \boldsymbol{y}\|^2, \tag{21}$$

with $\boldsymbol{x}_{cal}$ being the calibration data derived using the methodology stated above.

Unlike the chosen RTI model, each link is weighted equally, this was done due to its computational simplicity and adaptability to the inevitable elimination and ignoring of bad data links.

When a frame is captured it is compared to each one of the "expected value" frames from the calibration set. The location that has the smallest difference between expected value and measured value is chosen. It should be noted that the Radio Map model gives it's decision as a specific location within the WSN. This is in many ways a discretization of location. While RTI is of course discrete in nature, the localization image produced doesn't give a binary output for each location. It delivers a subjective image, from which further decision logic is required to decide if a subject is present at the location and where they are specifically within the WSN. The Radio Map model utilized within this experiment delivers a decision stating that a subject exists within a specific region, and is either correct or incorrect based off of the actual location of the subject.

Accuracy and Resolution of Radio Map Model.

As noted in the previous section, the Radio Map model delivers a specific chosen location from its list of calibrated locations as it's output. It is important to note

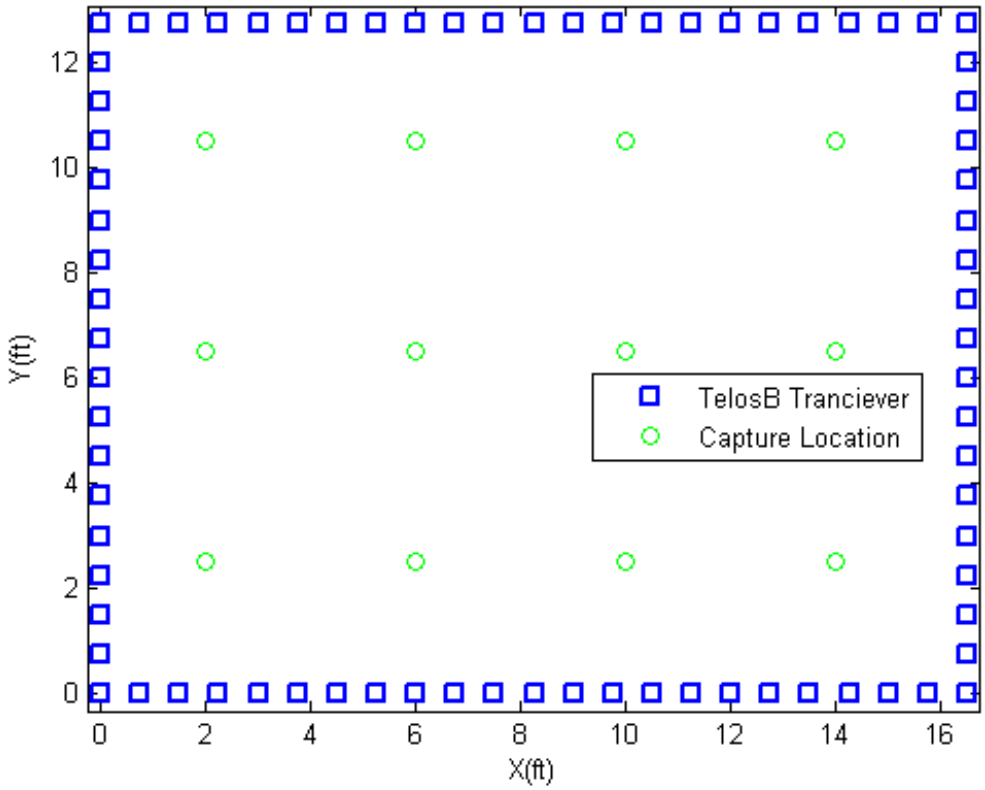

Figure 4. Layout of 78 mote WSN with mote and capture locations denoted

however that each one of these locations are actually just pixels, and that the physical location of the subject is simply decided to be within the chosen pixel. While the accuracy of these decisions may be very high, at 12 calibrated locations the resultant resolution is actually a roughly 16 square foot area. See Figure 5 for a visual explanation of this in practice.

Dealing with bad data sets.

In any given frame of data taken from the WSN described and imaged above, there is a very high chance, almost 85% in this experimentation, that at least one of the 78 telosB motes will fail to report its links to the base station. Matlab reads in these values as *nan* or Not A Number. Significant effort was made to reduce the

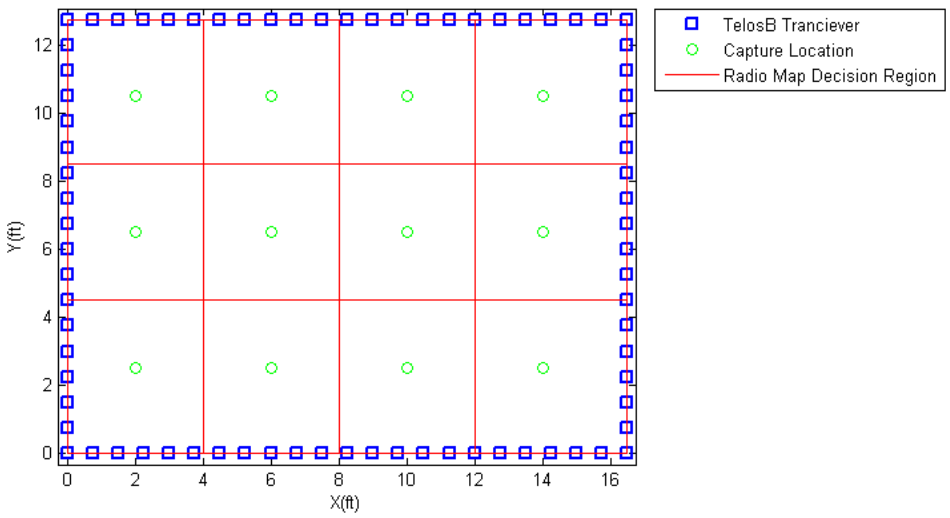

Figure 5. Image of 78 mote WSN with Radio Map decision region denoted

number of data sets containing bad links, however the floor for data sets containing at least one bad link for this experimentation is 65%. Due to the inevitable presence of bad links within any data set, a process was created to deal with them.

For RTI systems three possible approaches towards dealing with nan data are:

1. Eliminate the data set from your calculations: while this may seem like the most straightforward approach, from a computational perspective it would require re-sizing and re-forming the weight matrix, a process that would be challenging to complete in real time.

2. Replace the *nan* with a numerical zero: while this is exceptionally simple to implement, it adds significantly more error into the system, as the link value was most likely different than zero.

3. Keep the last "good" data link from a previous frame, for use with the rest of the new data set: keeping the old data link isn't difficult from a computational standpoint, and while it does add some error to the ultimate image, using the last value is the best guess for the current value. Additionally given all data

sets were taken in stationary positions, the previous value is also the expected value.

Ultimately keeping the prior data link was chosen for execution in this experimentation, due to the fact that this experimentation doesn't cover movement, and the opportunity costs of the other two options were too high from a computational or accuracy standpoint.

For the Radio Mapping system these error values were simply ignored during all calculation. While this reduced the overall amount of usable data within the system, no significant impact upon decision quality was noted until the utilized data sets became very small. Since multiple frames were utilized in the calibration period, real values were created for each node, and only those links that were down for the imaging frame were affected and ignored.

3.3 Assumptions

The following is a list of several of the key assumptions made in this experiment:

1. The noise in both systems is Gaussian
2. Each transceiver, being manufactured identically, operates the same, with identical performance and noise
3. The true position of subjects within the WSN and the number of subjects
4. The targets are tall enough to obstruct the LoS plane of the WSN
5. There is always a single target within the WSN
6. Background noise is uniform across all data sets
7. Calibration data for the WSN is available and was taken over at least 20 frames of data

8. The posture of living, human subjects is standing upright
9. No noise reduction filters are used in experimentation
10. The attenuation of RSS is uniform across the localization object
11. The attenuation of RSS is uniform across affected pixels
12. The orientation of the transceivers is universal and constant through all data sets
13. The physical layout of the laboratory is kept as constant as possible throughout all data sets, so the multi-path environment is as similar as possible

3.4 Equipment

The equipment utilized in this experiment include: 79 Memsic TelosB TPR2400 transceiver motes, a computer operating Microsoft Windows 7, various structural materials, such as PVC piping, and a large number of USB cables for powering the network of motes. Software tools include: MATLAB, Cygwin, TinyOS, Spin, and an RTI LINK GUI produced at AFIT. The rest of this section discusses in detail the tools listed above.

TelosB TPR2400.

The Memsic TelosB TPR2400 transceiver is utilized in this experiment to generate the WSN. The TelosB mote is produced by Crossbow Technology Incorporated. The TelosB mote is an inexpensive open source radio that utilizes the TinyOS operating system. The radios can be powered either through the use of batteries or USB cables. USB cables were used to power the motes in this experimentation. The motes are highly customizable through programming via the USB port. 79 total TelosB motes

were used, 78 as transceiver nodes creating the network, with one mote used as the base station to gather the RSS values and store them in a computer. [32]

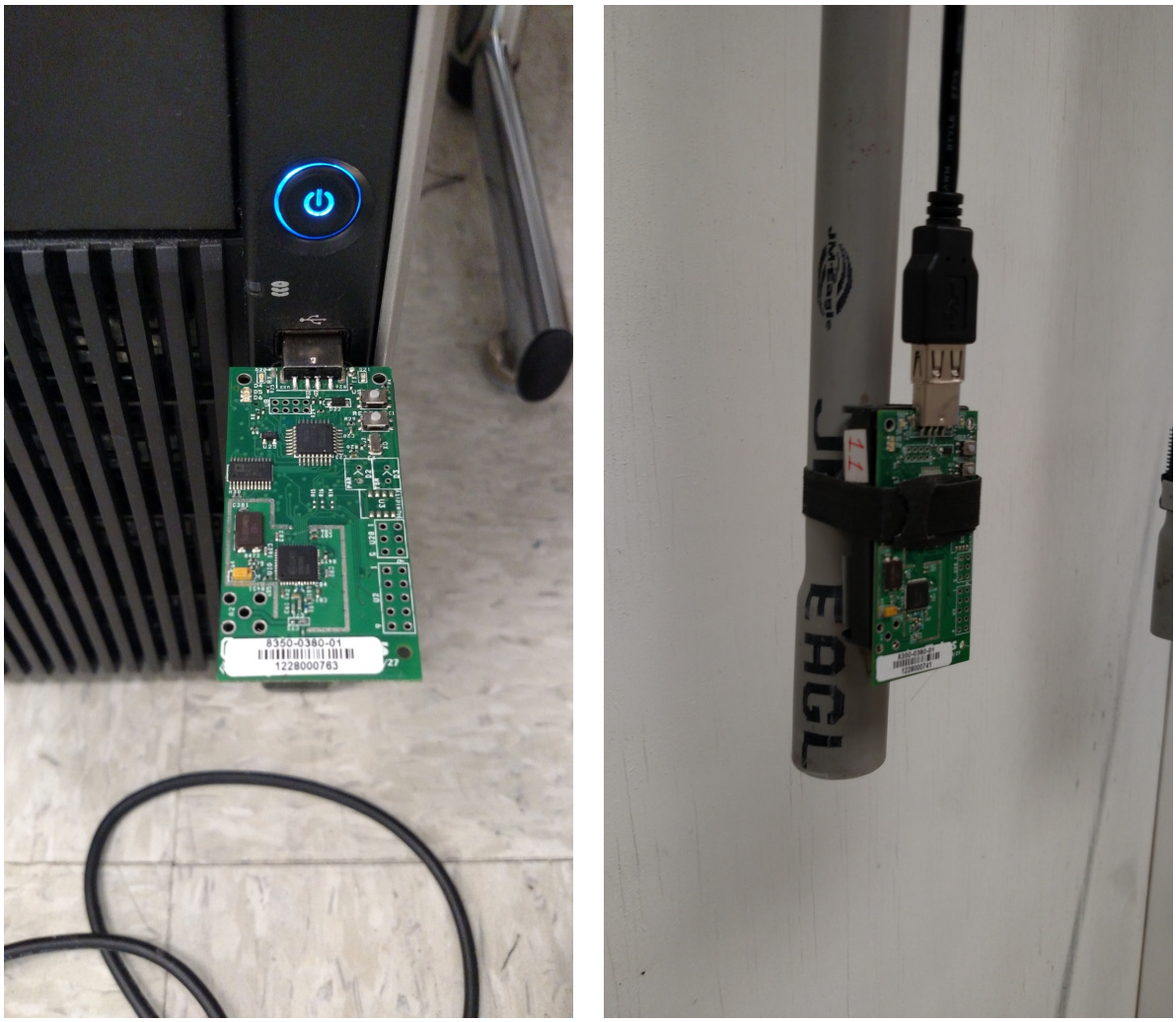

Figure 6. Picture of TelosB motes in both base-station and transceiver configuration

Cygwin.

Each mote was programmed using Cygwin. Cygwin operates similar to a Linux distribution on Windows by utilizing a large number of GNU and Open Source capabilities. It is currently owned and operated by Red Hat.

TinyOS.

TinyOS is an open source operating system utilized to program low power wireless devices. It was originally created at Stanford University. TinyOS is utilized in this research as the operating system of the the TelosB motes. [33]

Spin.

Spin is an open source TinyOS program created by the University of Utah for use in TelosB motes. It is a protocol that gathers the RSS of a WSN by utilizing token passing. The creators of Spin have specifically used it with TelosB motes. Spin ensures that only one mote transmits at a time, enabling all the other motes to gather and record the RSS data.

RTI LINK GUI.

The RTI LINK GUI is the final part of the data chain. Developed by Alex Folkerts, Tyler Heinl, and Dr. Richard Martin, it is a Matlab Application that collects, displays and saves data from an RTI network.

3.5 Localization Subject

For the data presented in this research a foam block pillar was used as the localization subject, it was chosen as the primary subject due to its uniformity and ease of use. Since it is an inanimate object there is zero undesired movement between data captures, making the only difference in data frames due to noise, or by experimental design.

3.6 Network Setup

A total number of 78 TelosB Transceiver motes were arranged according to Figure 4 to create a WSN that was 12.75 feet wide and 16.5 feet long. The motes were set at a height of 4 feet. The motes were spaced 0.75 feet apart from each other. See Figure 7 for a top down view of the mote layout and Figure 9 for a photograph of the WSN and greater laboratory. The reason for the unorthodox size and spacing of the WSN was due to safety concerns of the laboratory. In order to make any possible evacuation easier and limit the tripping hazard of roughly 1000 feet of USB cable, trays were hung from the ceilings. The motes and PVC pipe were hung from these, see Figure 8 for an image of this. The shape and spacing of the WSN were dictated by the layout of these trays in the laboratory.

The 78 motes included in the WSN were programmed utilizing TinyOS through the USB port. After significant trial and error, it was determined that up to 10 unique TelosB motes were programmable at a single time. To minimize confusion and error, the motes were programmed after they had been placed in their proper position on the WSN perimeter. For each of the 8 programming sessions, 100 feet of USB cable was run to a single USB hub which was then accessed by a laptop. After the 78 motes making up the WSN were programmed, the base station was finally programmed and plugged into a nearby Windows 7 desktop computer that was utilizing SPIN and the RTI LINK GUI. After programming, the USB cables connecting to each of the TelosB motes remained connected and were plugged in HUB drawing power from a standard 125 volt American wall outlet. This supplied power to the TelosB motes which are operable via both USB and AA battery. To ensure a steady power flow and reduce hassle in constant replacement, only USB power was used in this experimentation.

In an effort to maintain consistency, every TelosB mote was oriented with the USB port up, to allow easy access to the USB port from the cable trays. Additionally,

while the TelosB motes are equipped with an omni-directional antenna, each mote was positioned so that the same side, that of the printed circuit board, was facing towards the center of the WSN.

Utilizing equation (1) from Chapter II, we can calculate that the number of unique links generated by utilizing the full 78 mote network is:

$$U = (78^2 - 78)/2 = 3003 \tag{22}$$

Every data capture session utilized all 78 motes. During data processing we were able to pair down the data set, only utilizing the desired motes in calculation. The specific mote numbers utilized in calculation and comparison are discussed in the experiment design section later in this chapter.

3.7 Experimental Design

A total of 837 data sets were taken across 12 unique points within the WSN. This data was captured utilizing a foam pillar at all 12 locations. All data presented in this thesis was taken sequentially with minimal amount of time between sets. This was done in a effort to make uniform the position of each individual sensor across all data sets. This uniformity and brevity of duration also allows for a similar overall layout of the background lab and any background noise at time of capture.

The capture and calibration process for the foam block tests included the following steps:

1. Set up WSN turning on all motes and the PC utilized to capture data.

2. Turn on motes within WSN allowing a significant "handshaking period" of roughly 100 frames to automatically run, in order to minimize packet loss.

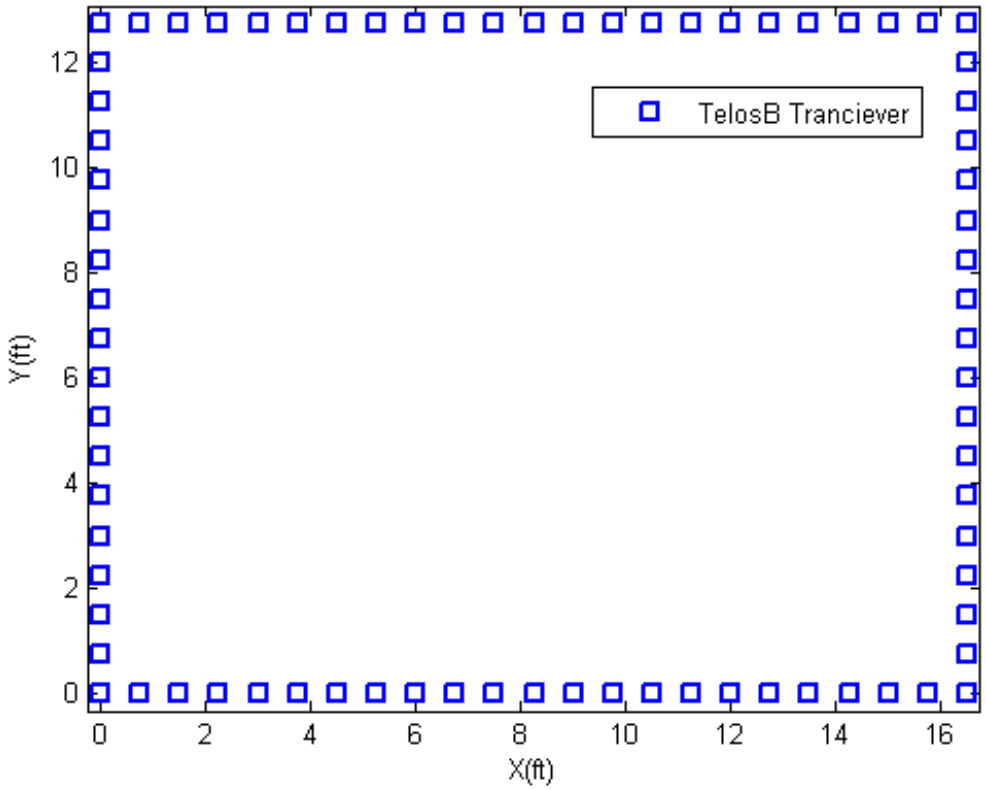

Figure 7. Image of 78 mote network set up

3. Clear WSN of any subjects and begin basic calibration of zero-obstruction RSS for WSN over a series of 20 frames.

4. With calibration complete, place foam block at first capture point and proceed to capture.

5. Repeat previous step until data capture has been completed at every chosen capture point.

Every data capture set utilized all 78 motes within the WSN. In order to display the effects and capabilities of both Radio Mapping and RTI systems with a lower number of transceivers within the WSN, a program was generated to down select the data so that only the links containing a specific list of motes was utilized. This enabled

Figure 8. Picture of WSN hanging apparatus

production of WSNs of varying mote number and geometry without time consuming re-programming of motes or physical movement of the WSN. Additionally, utilizing data from the same capture session grants a uniformity of noise between geometries and sensor number data compilations.

Foam Pillar Comparison Compilations.

837 unique frames of data were taken at 12 locations with the foam block. The goal in capture was to gather at least 60 frames at each location, 10 being used for calibration of the radio map and the remaining 50 used for data analysis. In practice the data sets for each location varied from a low of 62 frames to a high of 81 frames at a single location. For every frame captured an RTI image was produced. To enable easy comparison of RTI and Radio Mapping systems, both the actual location of the subject and the decision area output of the Radio Mapping model chosen were superimposed on the grayscale RTI image.

Figure 9. Picture of entire WSN and floor grid in lab

In addition to the original images produced using 78 motes, a new program was fabricated to down-select the links from the output file of the RTI LINK GUI so that images of a 39 mote WSN RTI system could be produced and compared to the resultant regions of decision in a Radio Mapping system. The data was then further down-selected to generate a 20 mote network with unique imagery for that network.

Down-selection of Data.

A program was generated to down-select the data acquired in the aforementioned data run, allowing the selection of a variable number of motes from the original 78, to generate a WSN of varying number and geometry. To view an accurate comparison between RTI and Radio Mapping as the number of motes within an WSN decreases, the WSN data was compiled at 39 and 20 motes, maintaining a rectangular geometry. See Figures 11 and 12 for visual depictions of their respective WSNs.

In order to properly down-select the data, the matrix of values must be decimated

Figure 10. Picture of foam pillar localization subject within WSN

in such a manner that the RSS values relating to links no longer within the WSN are eliminated. This was done by labeling the links with their respective motes, and eliminating any link who's respective motes were not included in the new WSN. Then the entire process of RTI, as outlined in chapter II, begins again with recompilation of the weight matrix, regularization and image production.

3.8 Metrics

Determining proper metrics for a side by side comparison of RTI and Radio Mapping systems presents a unique challenge. As stated above, the result of the Radio Mapping system utilized in this thesis is a location region chosen from a limited set, similar to a digital output, giving a "pixel" that the the target is determined to be located within. No noise is given in the output of this system. Therefore, the Radio Mapping system used within this thesis can only be measured by whether it is "correct" or not. In contrast to Radio Mapping, the output of an RTI system

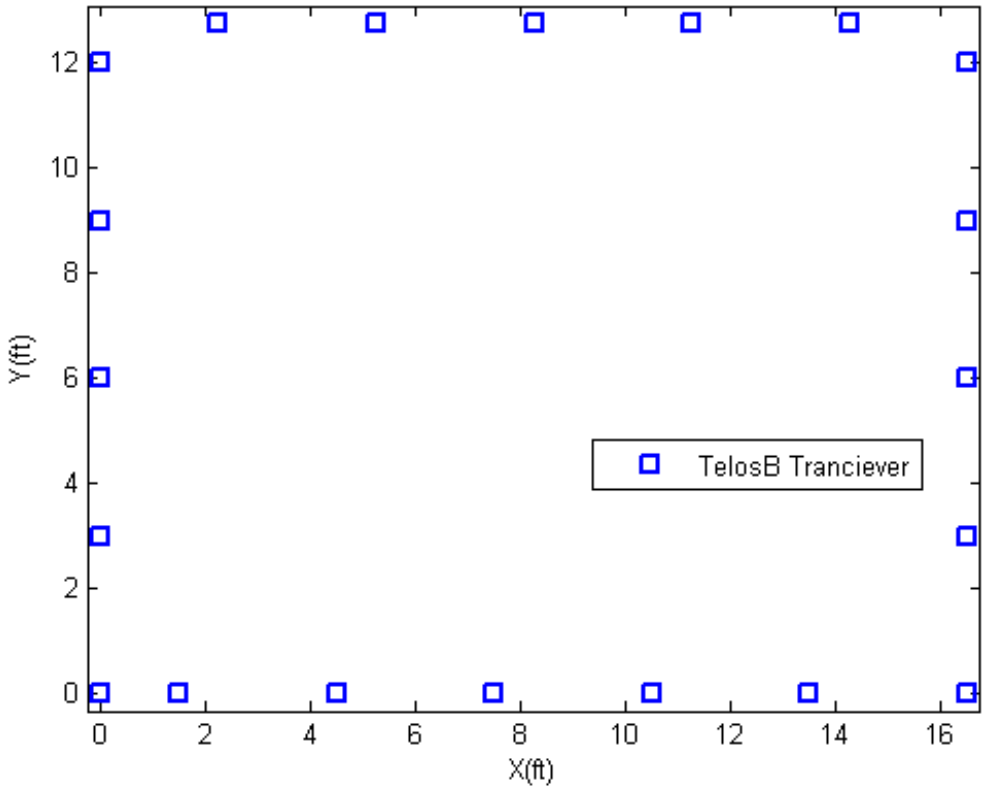

Figure 11. Image of WSN in 20 mote configuration, note offset motes in bottom left hand corner

appears almost analog. While it is still obviously digital in nature there is a significant amount of noise in the resultant gray scale image. RTI doesn't output an exact "decided" location that can be easily compared to Radio Mapping. In an effort to concisely compare these two systems, the resulting images are presented overlapping each other. The decision region for Radio mapping is outlined and placed over top of the resultant RTI image, with the actual location of the subject within the WSN marked.

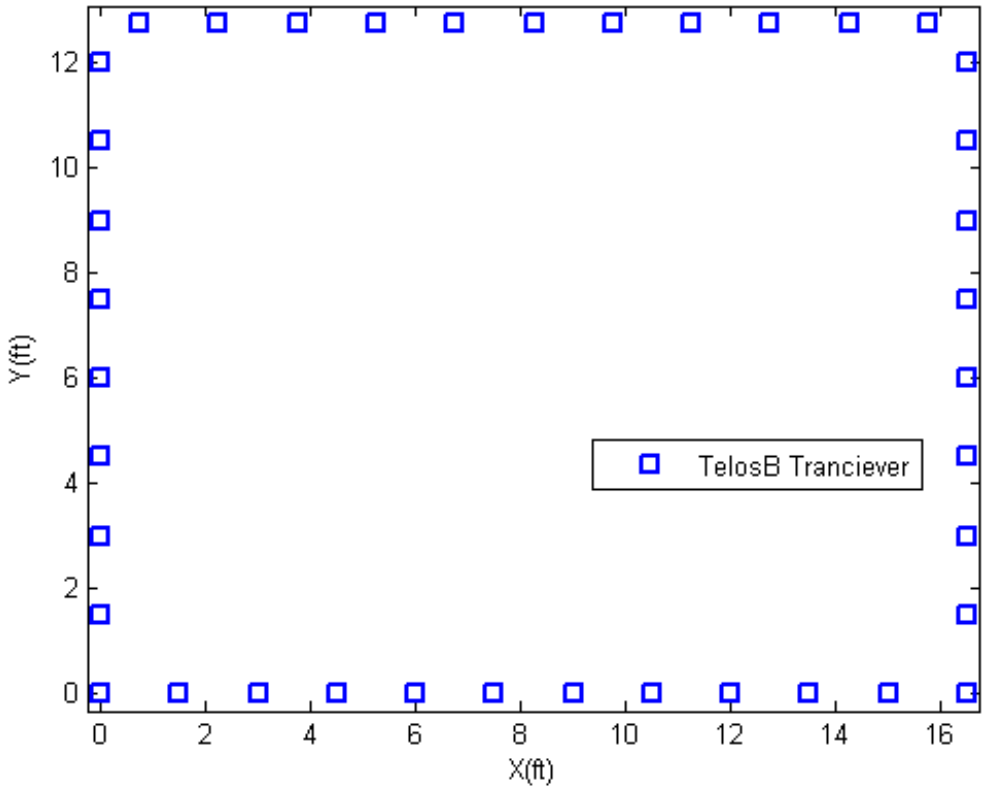

Figure 12. Image of WSN in 39 mote configuration

3.9 Conclusion

This chapter described in detail the methodology of the experimentation within this thesis. It began by outlining the goal of experimentation, focusing on a side by side comparison of RTI and Radio Mapping DFPL systems. It then declared the chosen models for those respective systems that were outlined in the previous chapter. Key assumptions made throughout experimentation were then identified. The hardware and software utilized were described, as well as the properties of the WSN utilized. Finally the experiment design and procedures were outlined, and the issue of metrics addressed. The following chapter presents the results of the experimentation described in this chapter and discusses those results.

IV. Results and Discussion

This chapter presents and discusses the results of the experimentation outlined in chapter III. Images from networks of equal size with 78, 39 and 20 motes arranged along the perimeter, are compared to the decision region of the Radio Mapping model. The compiled accuracy, results and limitations of Radio Mapping are discussed in detail, with comparisons drawn to the RTI results.

4.1 Radio Mapping Accuracy

The Radio Mapping methodology has the luxury of being able to be denoted as either "correct" or "incorrect" based on the decision region selected. If the capture location is within the decision region selected by the Radio Mapping methodology, then that decision can be considered correct. If the capture location exists outside of the decision region selected, then that decision is considered incorrect. Due to the digital nature of this process, it is possible to compile the data for all frames captured. This section details the accuracy of Radio Mapping under the circumstances, and a side by side comparison with Radio Mapping and RTI is done in a later section.

78 Mote Network Accuracy.

Utilizing all 78 motes physically within the WSN and generating calibration data from 10 captured frames, the Radio Mapping methodology was 100% accurate in "correctly" determining the location of the localization subject across all frames in all capture locations.

39 Mote Network Accuracy.

The network was down-selected to include only 39 motes, utilizing data from every other mote within the WSN. When still utilizing a 10 frame calibration period, the accuracy was still at 100% across all frames and locations. At a reduced calibration period of 5 frames the Radio Mapping Model was still 100% accurate

20 Mote Network Accuracy.

The network was further down-selected to include only 20 motes, and again while still utilizing a 10 and 5 frame calibration period the Radio Mapping methodology was still able to correctly determine the location region 100% of the time.

Further Down-selection with Radio Mapping Methodology.

Even when the WSN was down-selected to 10 motes, if given a 5 frame period of calibration, the Radio Mapping model was still 100% accurate in localizing the subject. It should be noted that the RTI system was not tested at this level of down-selection, as the image quality had already broken down significantly.

It was only at a 5 mote WSN did incorrect outputs begin to manifest themselves within the Radio Mapping methodology. The lower limits on the number of sensors required in a Radio Mapping system was not the main drive of this thesis, and therefore was not investigated further.

4.2 RTI Accuracy

RTI performed as expected, with degradation of image quality as the number of motes within the WSN decreased. While 837 total images were captured only 18 are presented within this chapter, 6 from each of the network configurations, at 6 different points within that WSN. Due to the relatively symmetrical nature of the

WSN constructed, only frames taken from one side of the WSN are presented within this chapter. For additional frames from all locations see Appendix A, B and C for data from the 78, 39 and 20 mote networks respectively.

78 Mote Network Accuracy.

Utilizing all 78 motes in the physical WSN the RTI methodology is able to accurately predict the location of the subject. When the subject is close to the edges of the WSN the image quality is notably better than when the subject is moved towards the center of the WSN. This is due to a higher density of links that pass through these regions.

39 Mote Network Accuracy.

For 39 motes the image quality of the RTI image has degraded significantly. This is due to an exponential decrease in the number links within the WSN.

A similar effect of image quality in relation to positioning of the localization subject, relative to that of the 78 mote network was observed. What could be subjectively described as the highest quality image occurs when the subject is closest to the corner of the WSN. At this location the subject is properly localized. When the subject moves away from the corner the image quality begins to degrade heavily, along the side of the WSN it is still possible to localize the subject but the quality of the image and effective "signal to noise ratio" is reduced. When the subject is moved towards the center of the WSN, resolution of an exact location for the subject becomes very difficult, as shown in Figure 22.

It is at this point that the comparison between RTI and Radio Mapping starts to break down. The Radio Map methodology is still 100% accurate with a WSN of this size and disposition, at any location within said WSN. While RTI is still

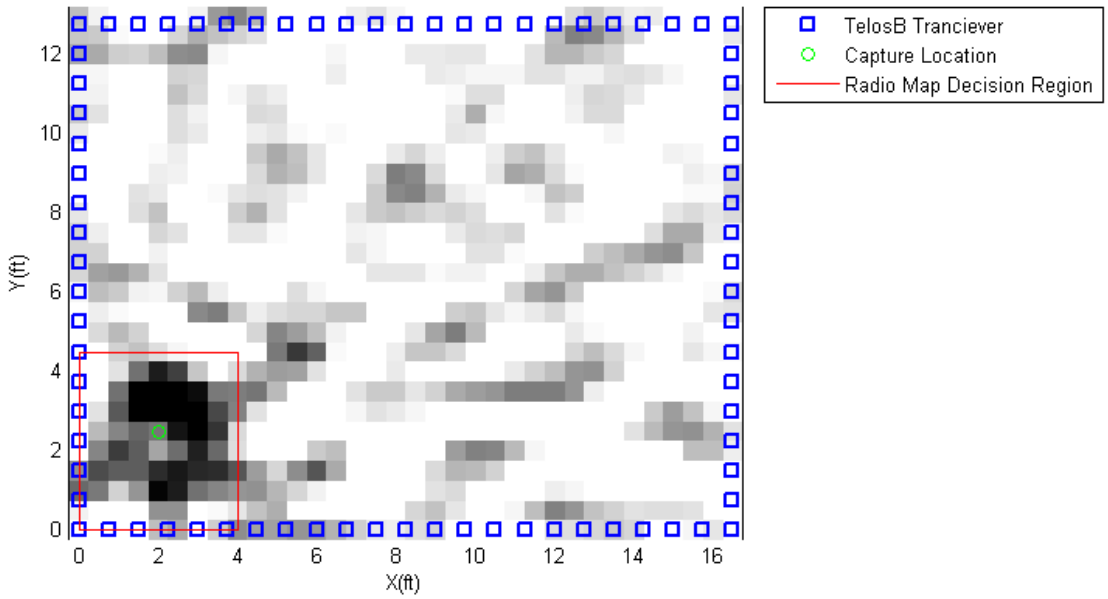

Figure 13. Image of 78 mote WSN with capture location at (2, 2.5) with Radio Map decision overlay

accurately able to locate the subject if it is located at the perimeter of the WSN, it struggles to present an acceptable image as the subject moves towards the center of the WSN. Significant post processing utilizing prior calibration may be able to deliver an accurate location for the subject, but that would eliminate arguably the greatest advantage of RTI systems over Radio Mapping.

20 Mote Network Accuracy.

For 20 motes, the imagery produced by the RTI system is less accurate and further "blurred" as there are only 190 unique links within the WSN. The same effect that occurred in the other two networks occurs to a greater extent here. The image could be subjectively determined "best" at the corner of the WSN with degradation as the subject was moved to the sides. Interestingly the image was remarkably good at the center of the WSN, better so than the 39 mote network, for the same exact frame. It was determined that the reason for a better image produced from seemingly less data

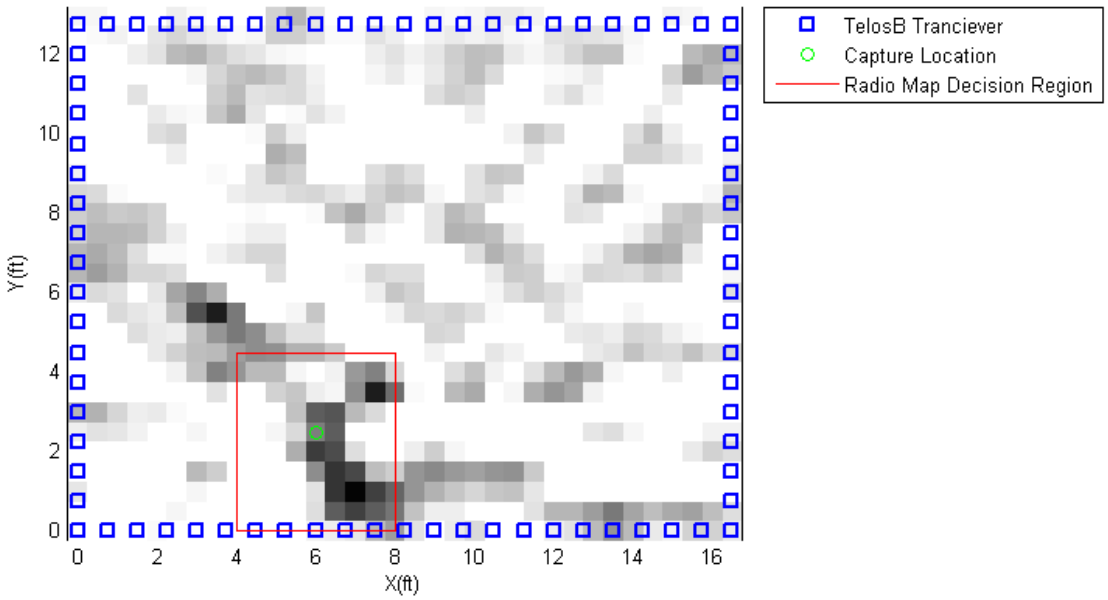

Figure 14. Image of 78 mote WSN with capture location at (6, 2.5) with Radio Map decision overlay

was simply coincidence that the links removed from the network that pass through the location in question must have had a higher multi-path or other noise modifier, resulting in a subjectively cleaner image when these links were removed.

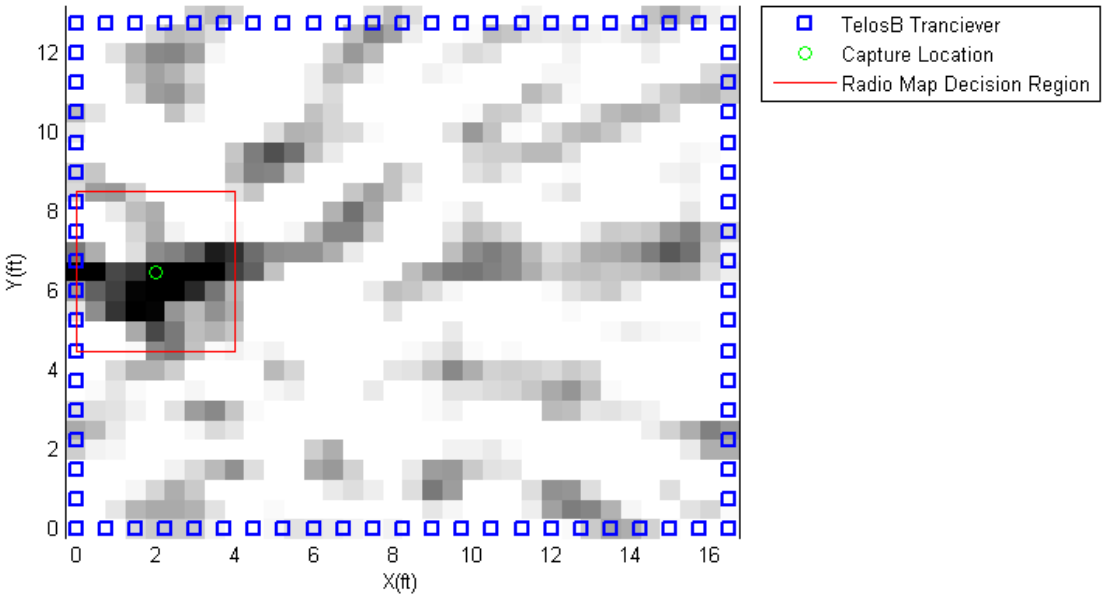

Figure 15. Image of 78 mote WSN with capture location at (2, 6.5) with Radio Map decision overlay

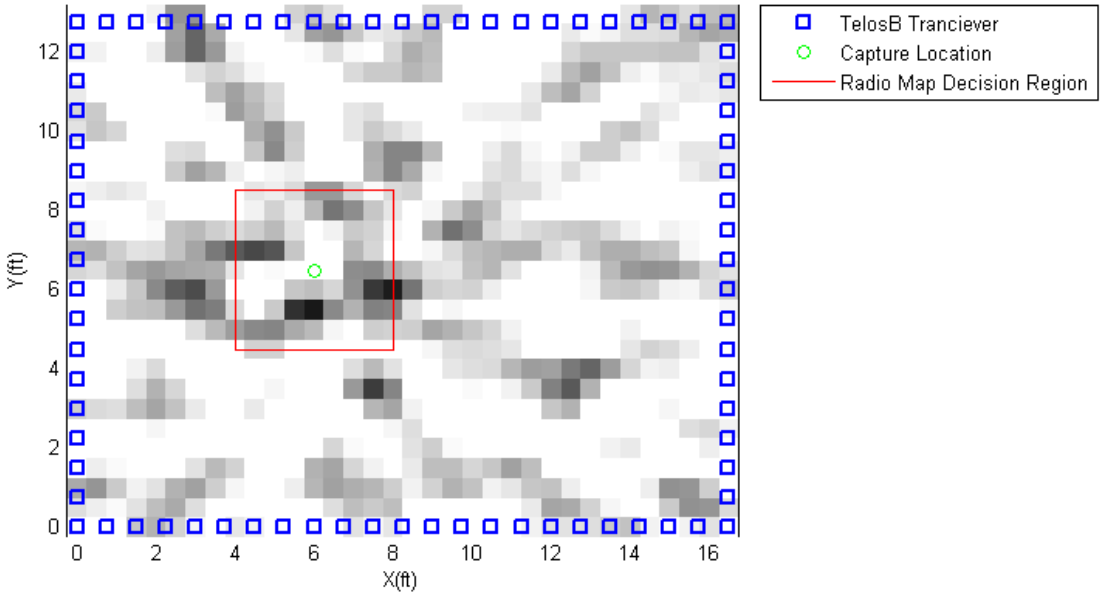

Figure 16. Image of 78 mote WSN with capture location at (6, 6.5) with Radio Map decision overlay

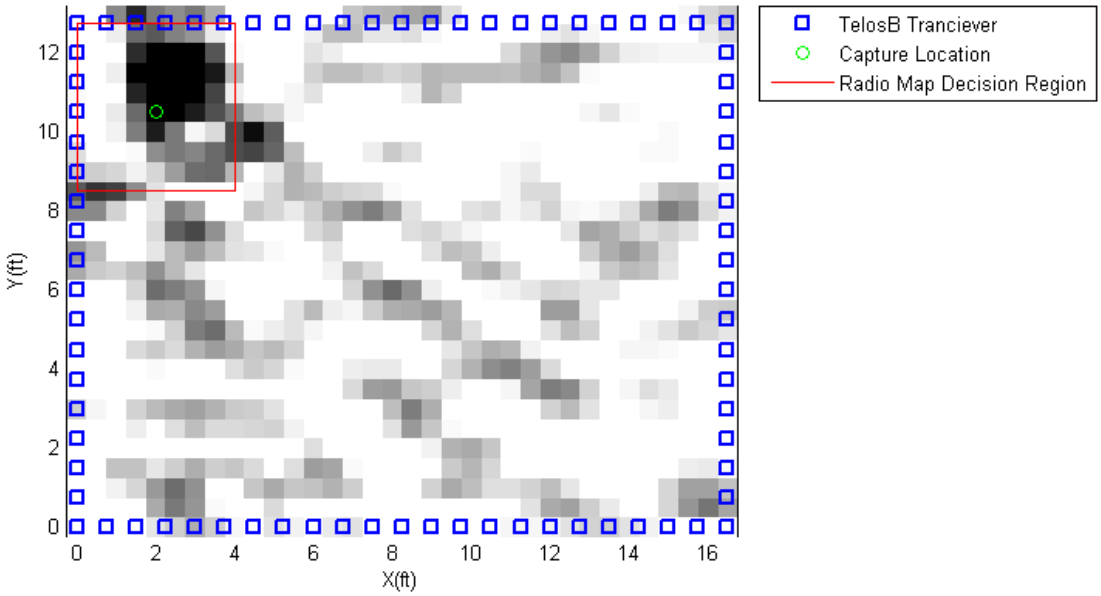

Figure 17. Image of 78 mote WSN with capture location at (2, 10.5) with Radio Map decision overlay

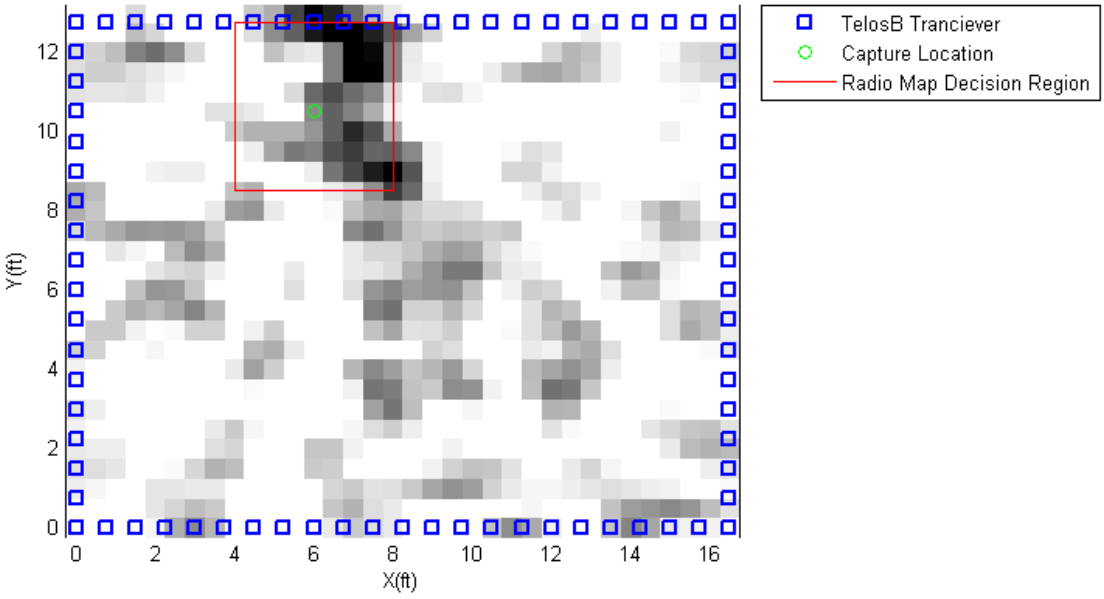

Figure 18. Image of 78 mote WSN with capture location at (6, 10.5) with Radio Map decision overlay

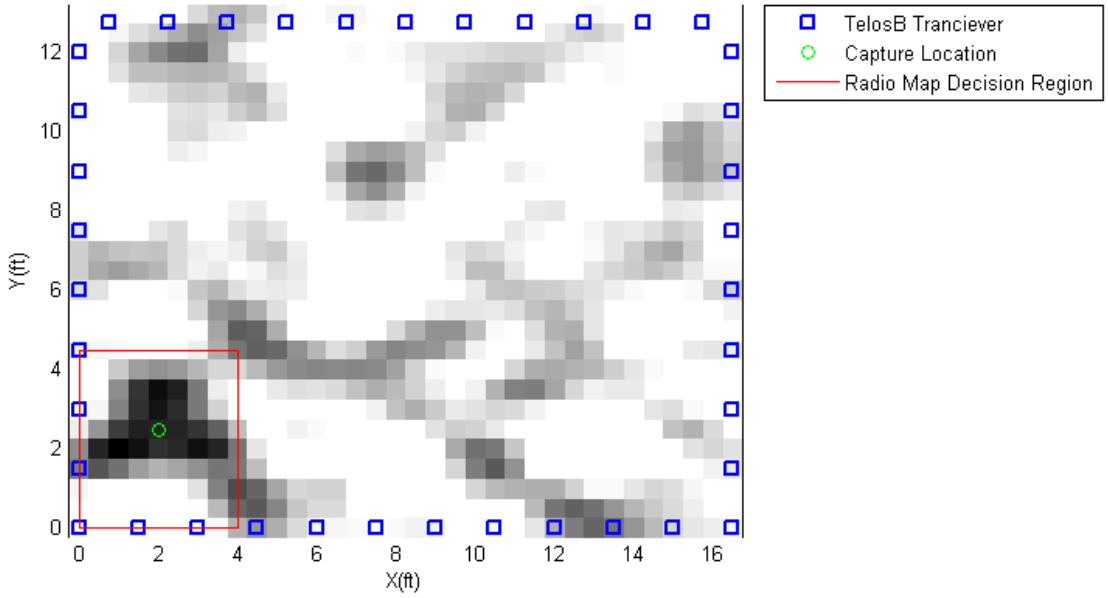

Figure 19. Image of 39 mote WSN with capture location at (2, 2.5) with Radio Map decision overlay

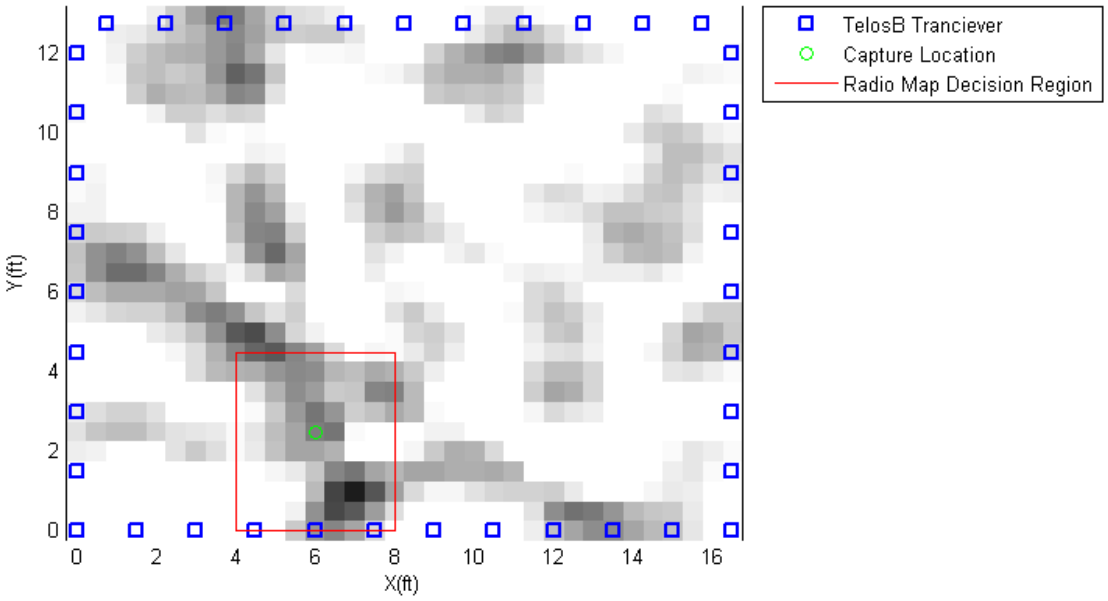

Figure 20. Image of 39 mote WSN with capture location at (6, 2.5) with Radio Map decision overlay

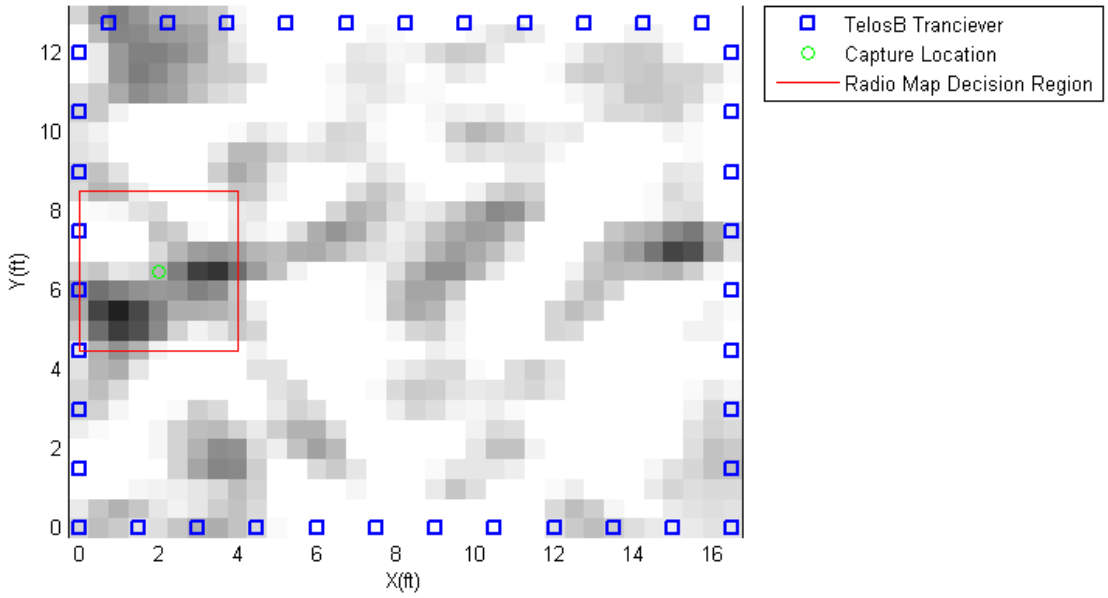

Figure 21. Image of 39 mote WSN with capture location at (2, 6.5) with Radio Map decision overlay

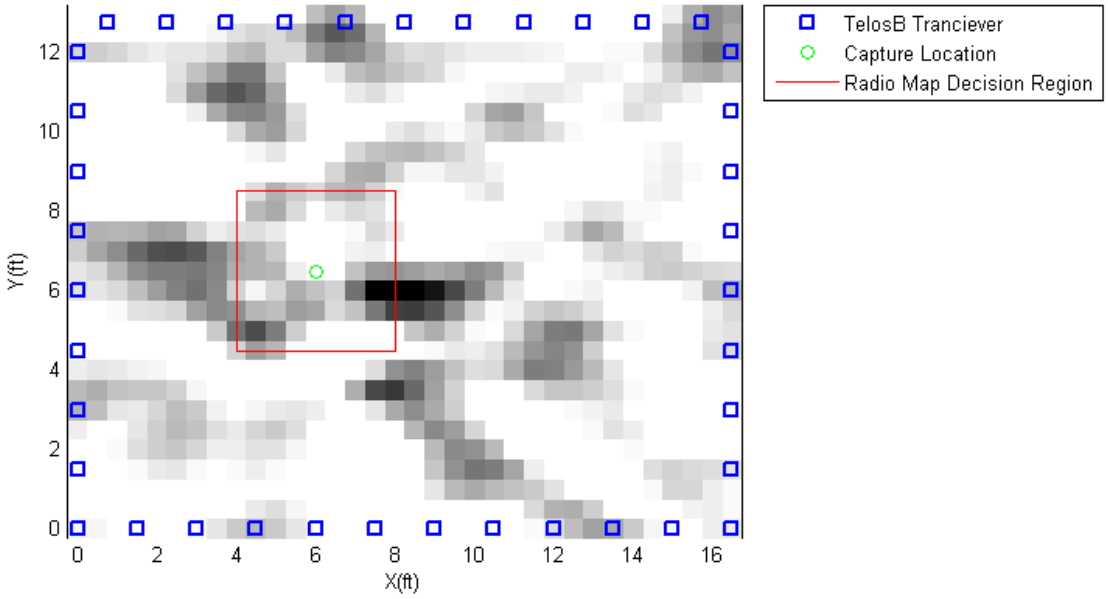

Figure 22. Image of 39 mote WSN with capture location at (6, 6.5) with Radio Map decision overlay

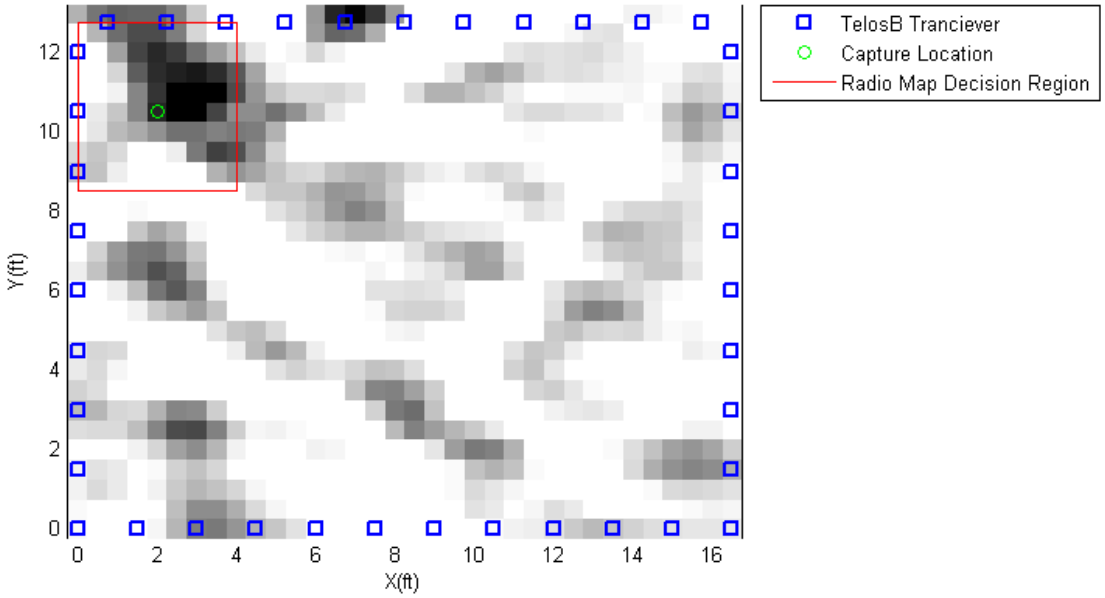

Figure 23. Image of 39 mote WSN with capture location at (2, 10.5) with Radio Map decision overlay

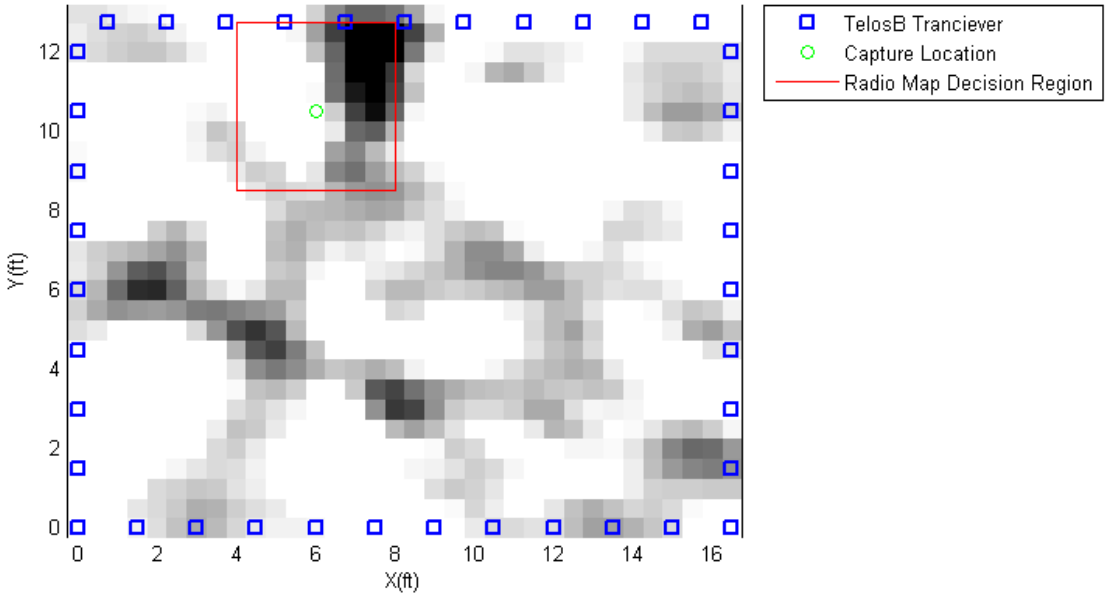

Figure 24. Image of 39 mote WSN with capture location at (6, 10.5) with Radio Map decision overlay

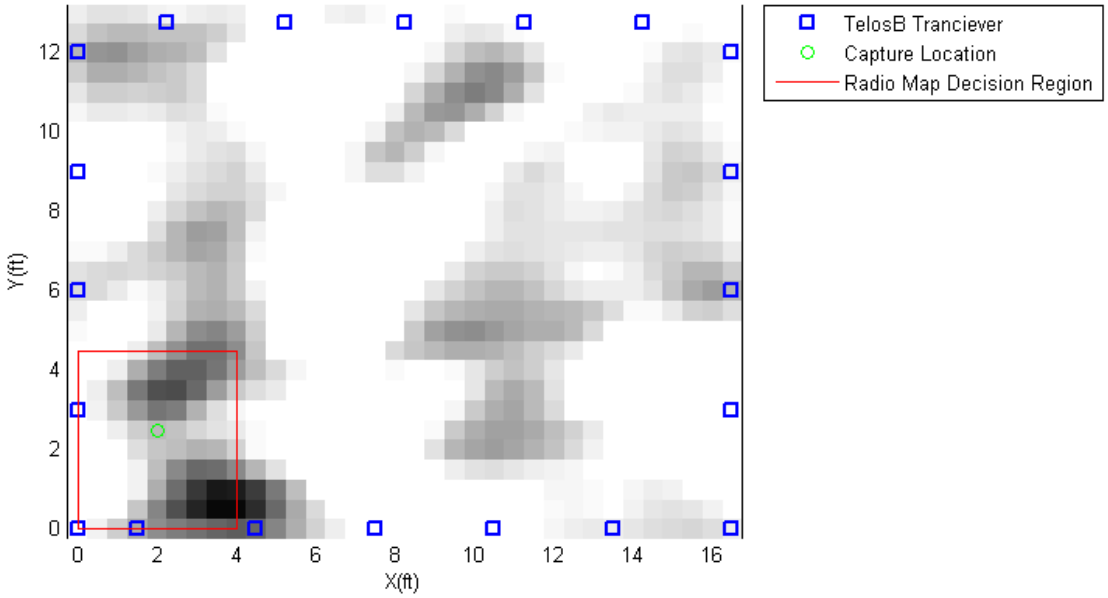

Figure 25. Image of 20 mote WSN with capture location at (2, 2.5) with Radio Map decision overlay

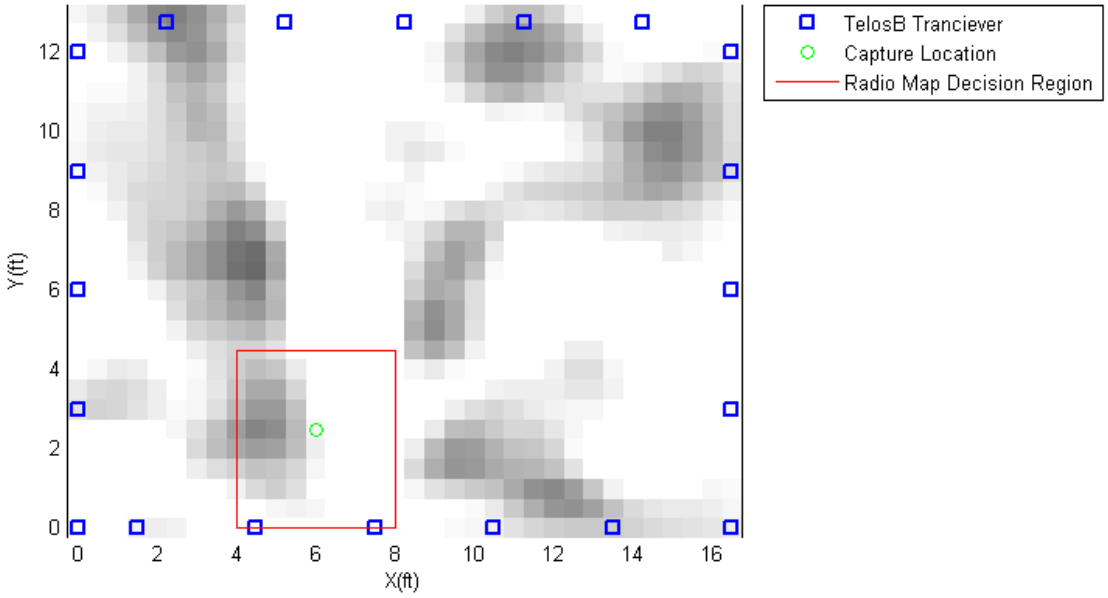

Figure 26. Image of 20 mote WSN with capture location at (6, 2.5) with Radio Map decision overlay

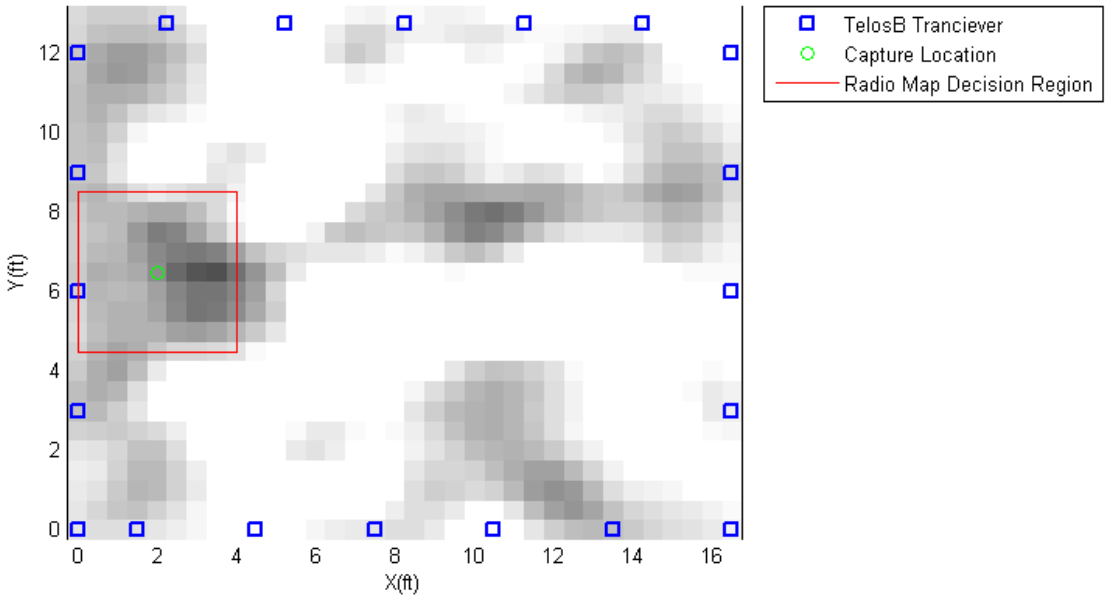

Figure 27. Image of 20 mote WSN with capture location at (2, 6.5) with Radio Map decision overlay

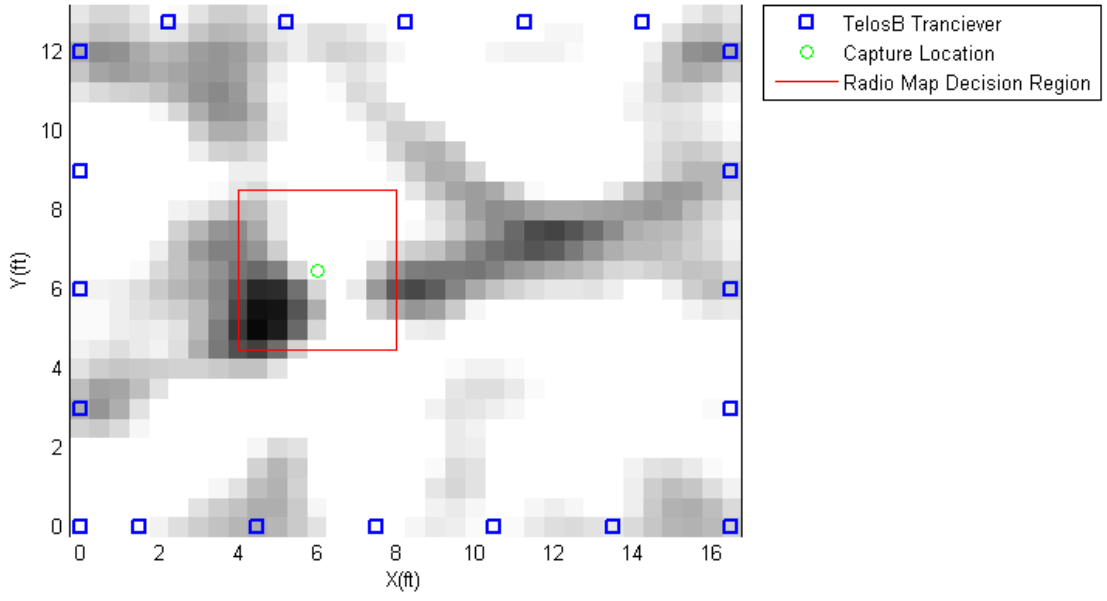

Figure 28. Image of 20 mote WSN with capture location at (6, 6.5) with Radio Map decision overlay

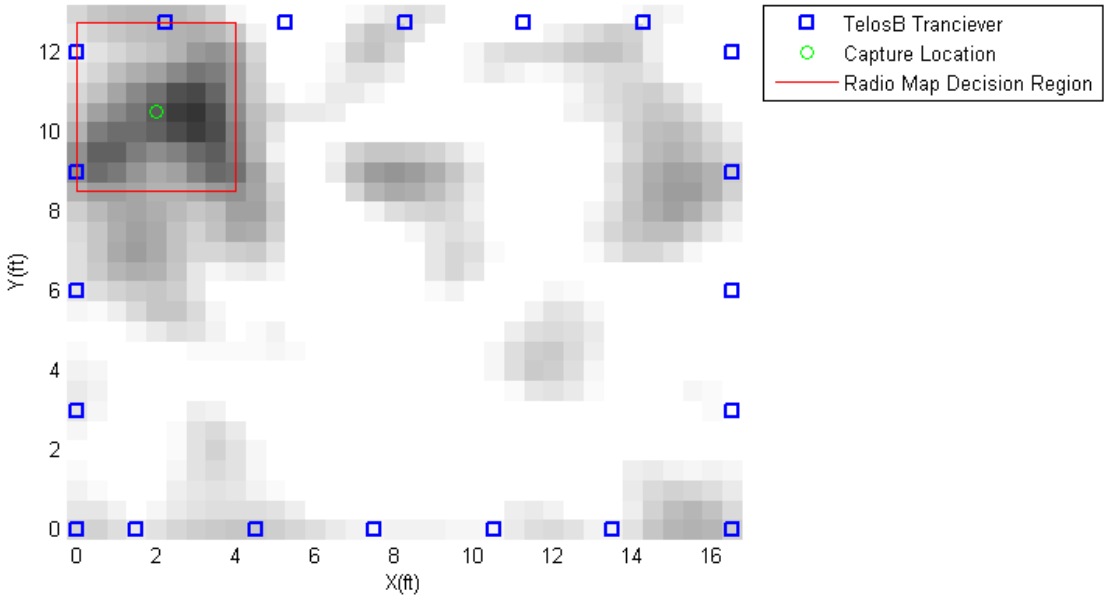

Figure 29. Image of 20 mote WSN with capture location at (2, 10.5) with Radio Map decision overlay

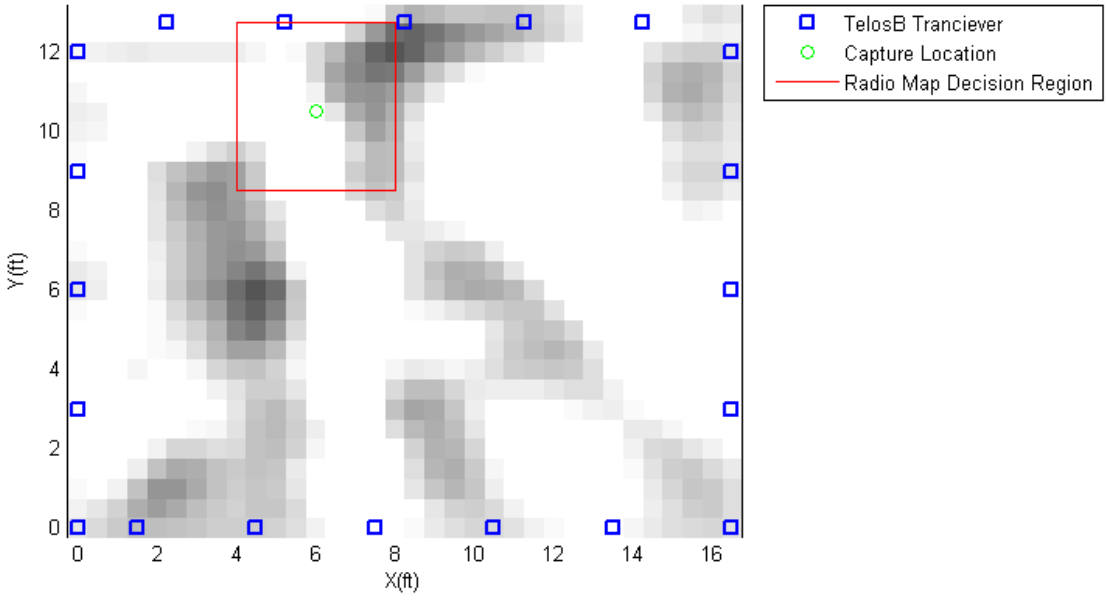

Figure 30. Image of 20 mote WSN with capture location at (6, 10.5) with Radio Map decision overlay

V. Conclusion and Future Work

This chapter summarizes the research and experimentation discussed within this thesis and recommends possible avenues for further research.

5.1 Summary and Conclusion

This thesis generated a side-by-side visual comparison of RTI systems and Radio Mapping. RTI is an upcoming and promising means of DFPL within a WSN utilizing TelosB transceivers, and Radio Mapping is a relatively unexplored means of localization within small scale WSNs. In chapter II, the prior work was discussed and an in depth look at the respective methodologies was detailed. In chapter III, the specifics of how the experimentation was conducted were discussed. In chapter IV the results and images produced by the procedure utilized were presented and discussed.

Within the parameters for which it was tested, Radio Mapping performed extremely well, being 100% accurate in all comparisons with RTI. However, it must be noted that the calibration complexity for a Radio Mapping system grows exponentially with both a desired increase of precision and robustness. For example, the Radio Map generated for this experimentation doesn't take into account the possibility of multiple subjects residing within the WSN and the possibility of there being no subject within the WSN. However, within the range of this experimentation Radio Mapping shows extreme promise, especially in WSNs with either a high multi-path environment, or with very few transceivers.

Results in this thesis compared to prior results of RTI systems contain a large amount of error. This may be due to high multi-path avenues within the laboratory, because upon inspection of the attenuation values for links passing through the subject, it was noted that a large percentage of links were simply not being attenuated

when they should have been. In WSNs containing a large number of transceivers the RTI methodology utilized is capable of properly localizing the subject. However, as the number of transceivers in the utilized WSN was reduced, the image quality was greatly reduced.

In summary, Radio Mapping and RTI methods of localization were proven to have unique weaknesses and strengths relative to each other. Radio Mapping proved itself as a potential means of localization within a prefabricated and properly calibrated WSN.

5.2 Future Work

Unique subjects within a pre-made Radio Map.

Introducing subjects that differ from the calibration subject could help test the robustness of the Radio Mapping methodology. RTI functions identically between subjects and is not adversely affected if a unique subject is introduced to the WSN.

Testing at points different from calibration points.

The localization subject was tested for Radio Mapping at the same location that the Radio Map was calibrated. Testing should be done to see how Radio Mapping performs if the localization subject is located at an un-calibrated point within the WSN.

Mitigation of multi-path signals in an RTI system.

Much of the issue with RTI in this experimentation was attributed to multi-path. While this issue is perverse, efforts to mitigate it's impact on an RTI system could improve the technology measurably.

Appendices

COMPARISON OF METHODS FOR RADIO POSITION OF NON-EMITTING DISMOUNTS

A. RTI Images of 78 Mote Network

This appendix contains an additional 24 images from the 78 mote network. Out of 837 frames, 2 were chosen at random from each calibration location and included in the figures below. In the interest of space, the legends and axis labels have been removed, but they are identical to the figures displayed in section 4.2.

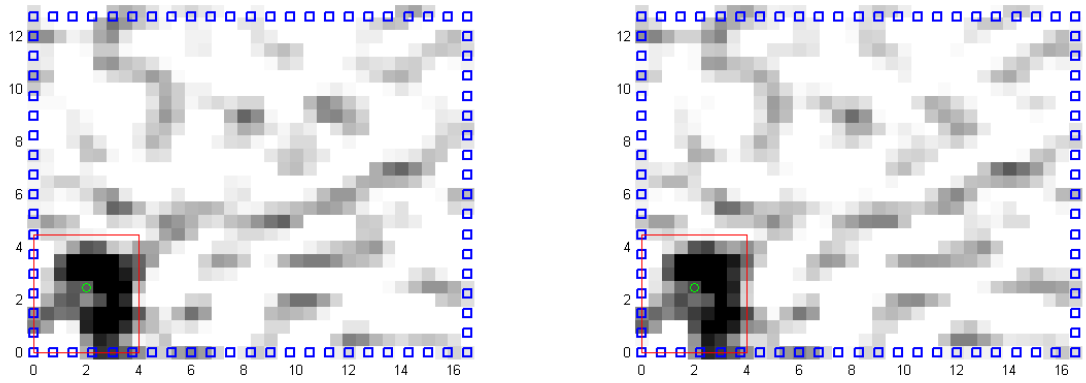

Figure 31. RTI image with Radio Map decision region for 78 motes location (2, 2.5)

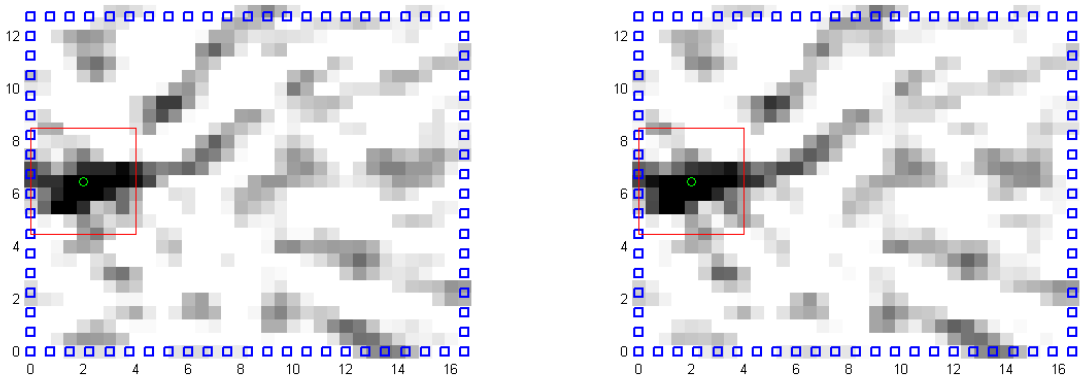

Figure 32. RTI image with Radio Map decision region for 78 motes location (2, 6.5)

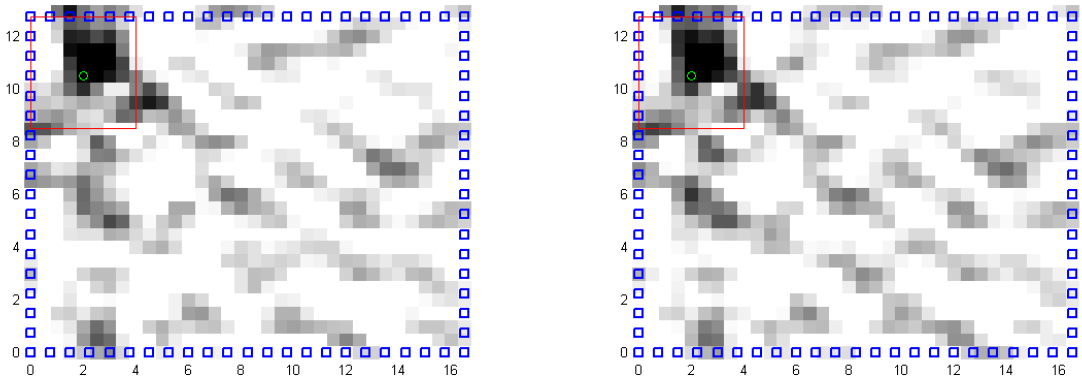

Figure 33. RTI image with Radio Map decision region for 78 motes location (2, 10.5)

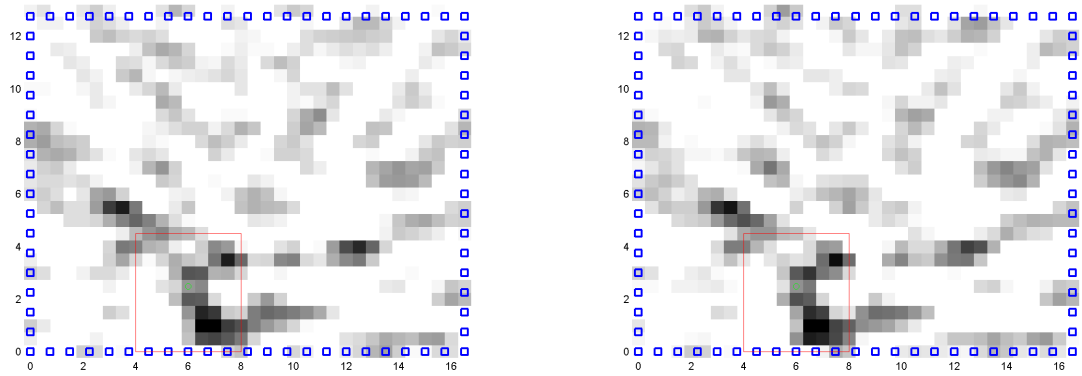

Figure 34. RTI image with Radio Map decision region for 78 motes location (6, 2.5)

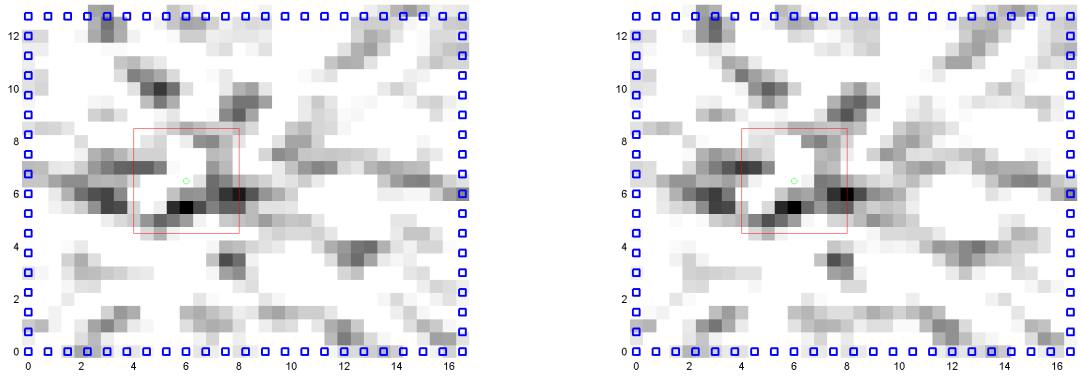

Figure 35. RTI image with Radio Map decision region for 78 motes location (6, 6.5)

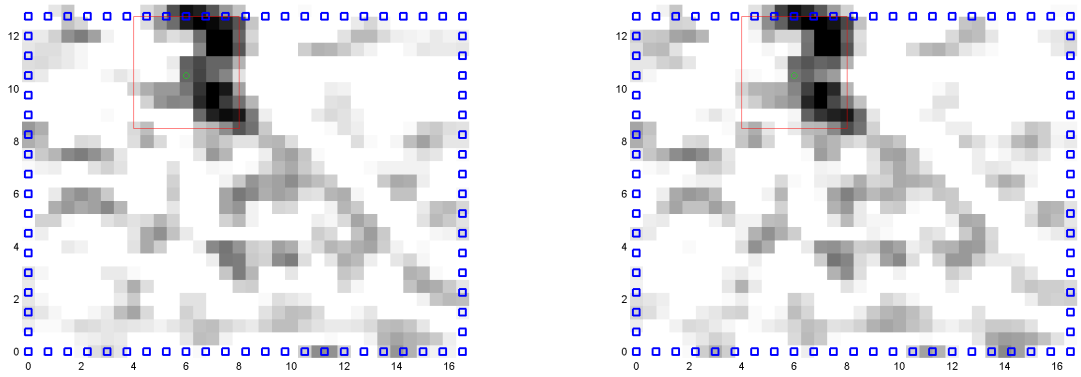

Figure 36. RTI image with Radio Map decision region for 78 motes location (6, 10.5)

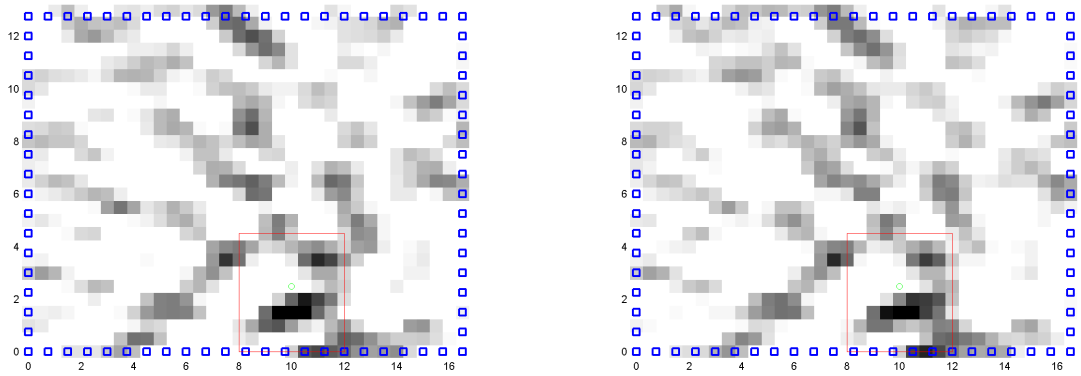

Figure 37. RTI image with Radio Map decision region for 78 motes location (10, 2.5)

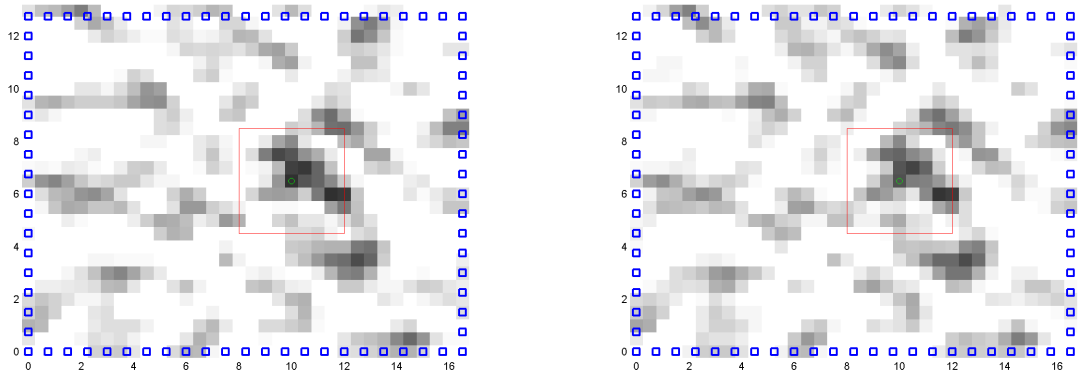

Figure 38. RTI image with Radio Map decision region for 78 motes location (10, 6.5)

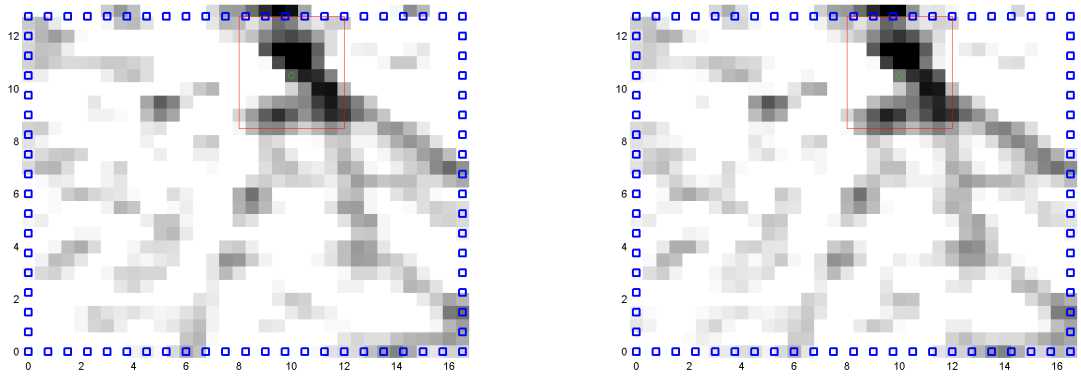

Figure 39. RTI image with Radio Map decision region for 78 motes location (10, 10.5)

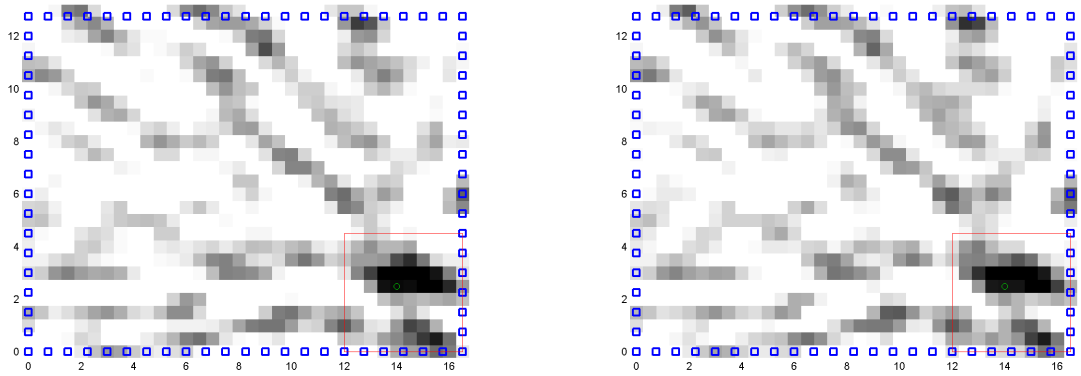

Figure 40. RTI image with Radio Map decision region for 78 motes location (14, 2.5)

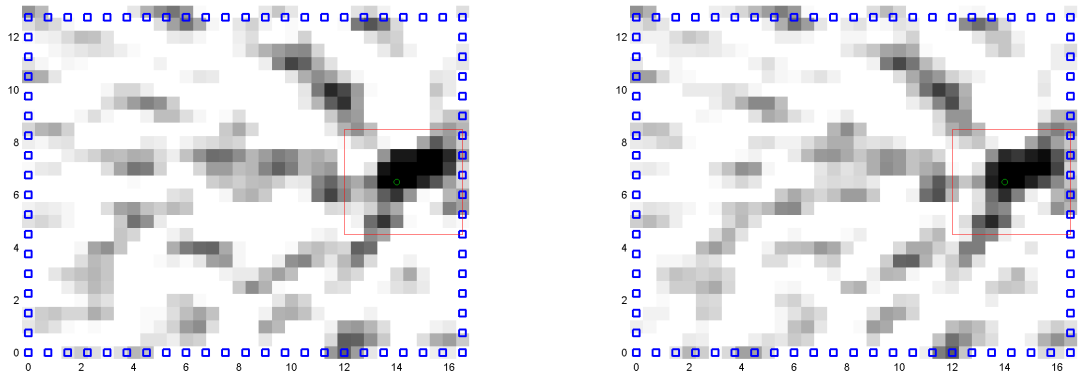

Figure 41. RTI image with Radio Map decision region for 78 motes location (14, 6.5)

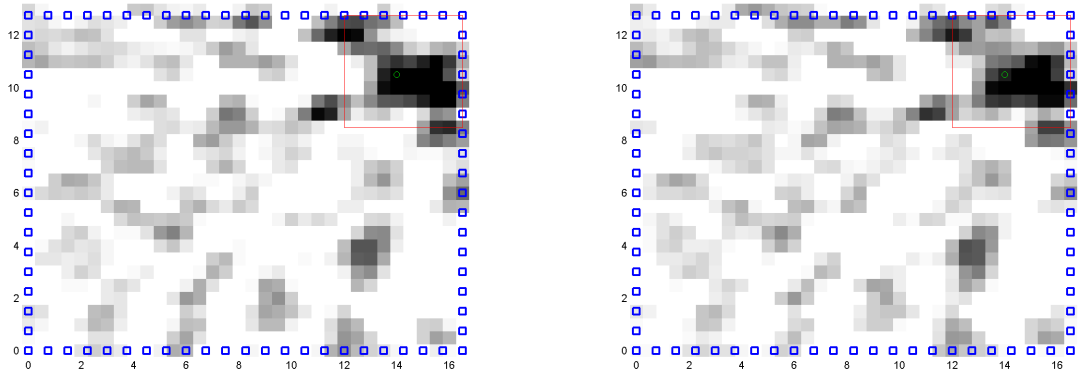

Figure 42. RTI image with Radio Map decision region for 78 motes location (14, 10.5)

B. RTI Images of 39 Mote Network

This appendix contains an additional 24 images from the 39 mote network. Out of 837 frames, 2 were chosen at random from each of the 12 calibration locations and included in the figures below. In the interest of space, the legends and axis labels have been removed, but they are identical to the figures displayed in section 4.2.

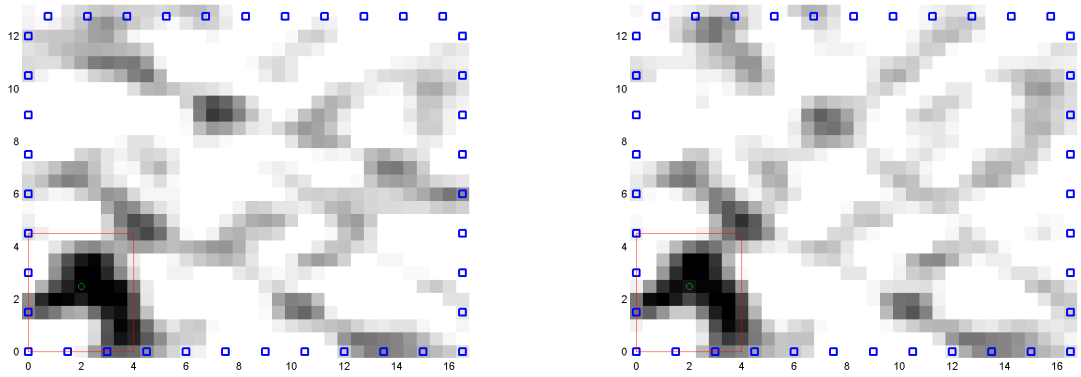

Figure 43. RTI image with Radio Map decision region for 39 motes location (2, 2.5)

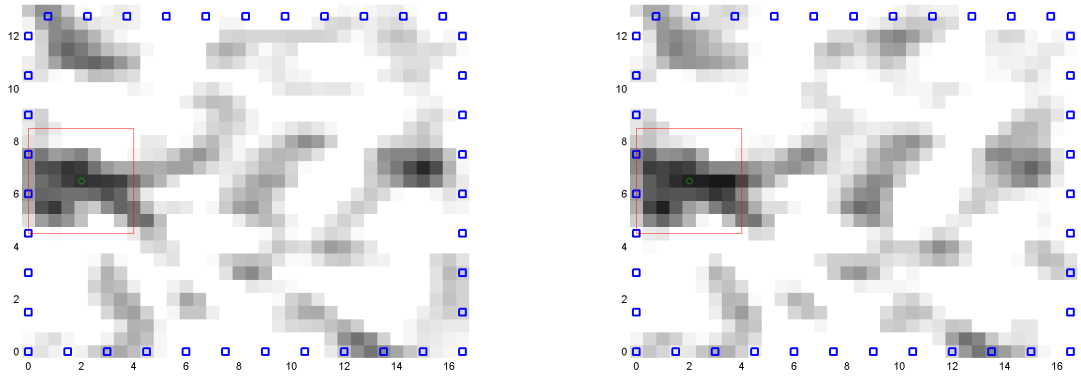

Figure 44. RTI image with Radio Map decision region for 39 motes location (2, 6.5)

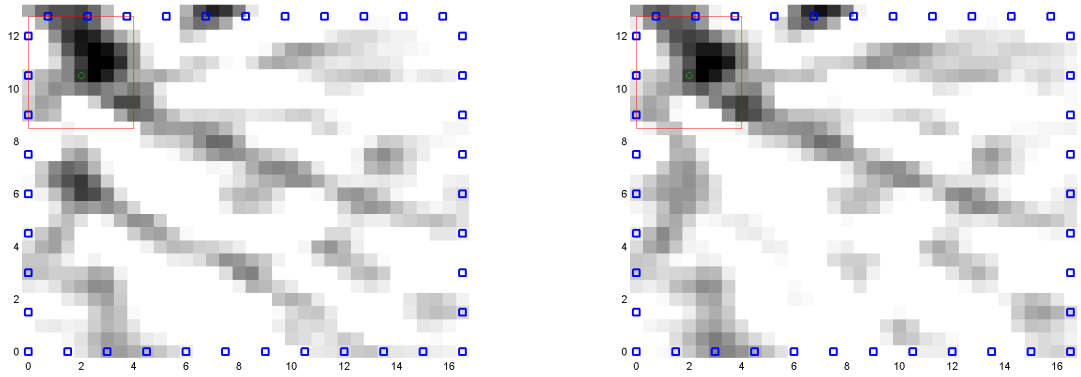

Figure 45. RTI image with Radio Map decision region for 39 motes location (2, 10.5)

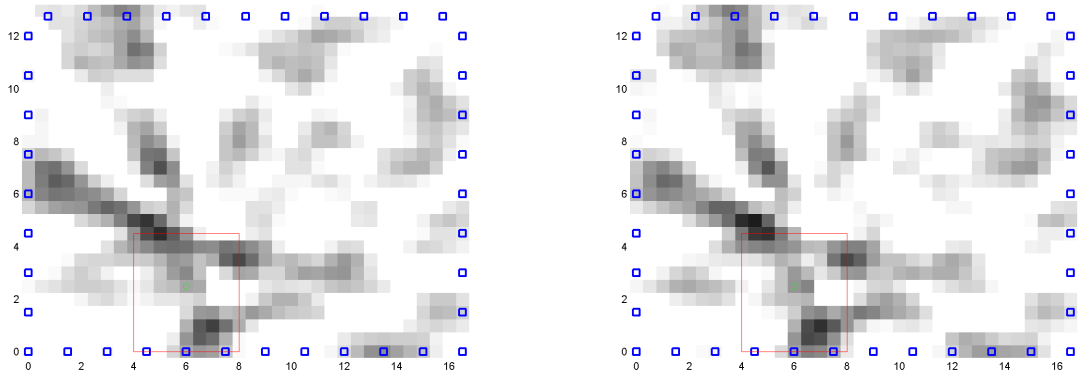

Figure 46. RTI image with Radio Map decision region for 39 motes location (6, 2.5)

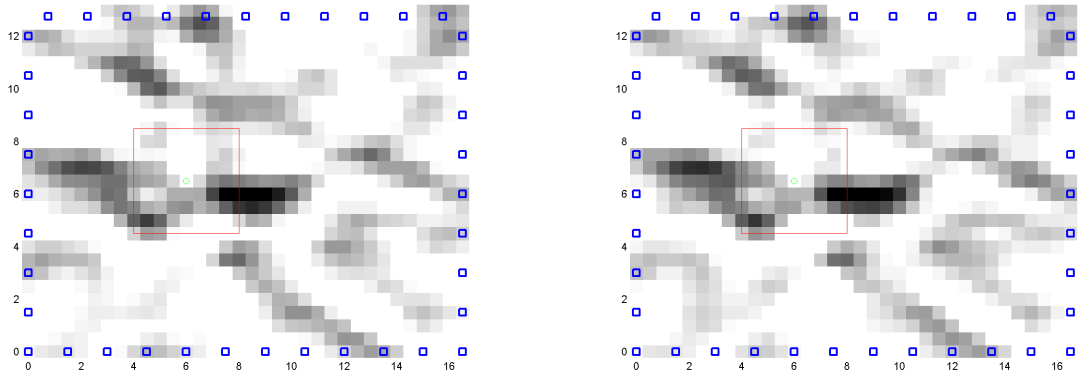

Figure 47. RTI image with Radio Map decision region for 39 motes location (6, 6.5)

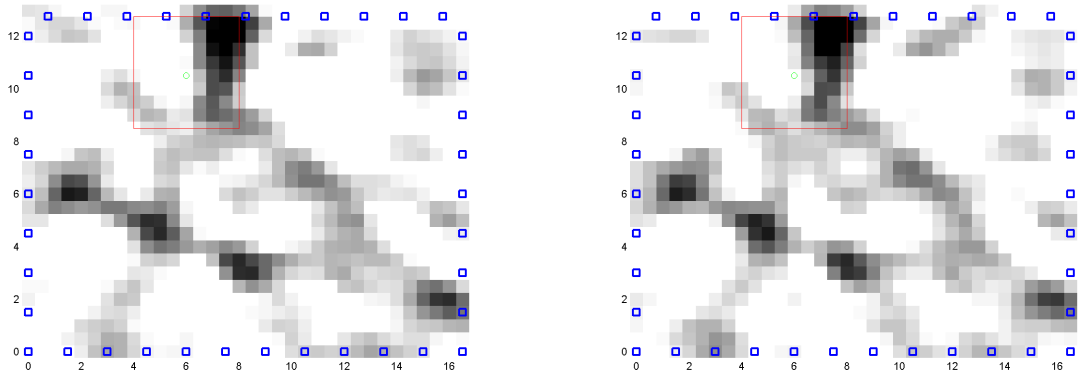

Figure 48. RTI image with Radio Map decision region for 39 motes location (6, 10.5)

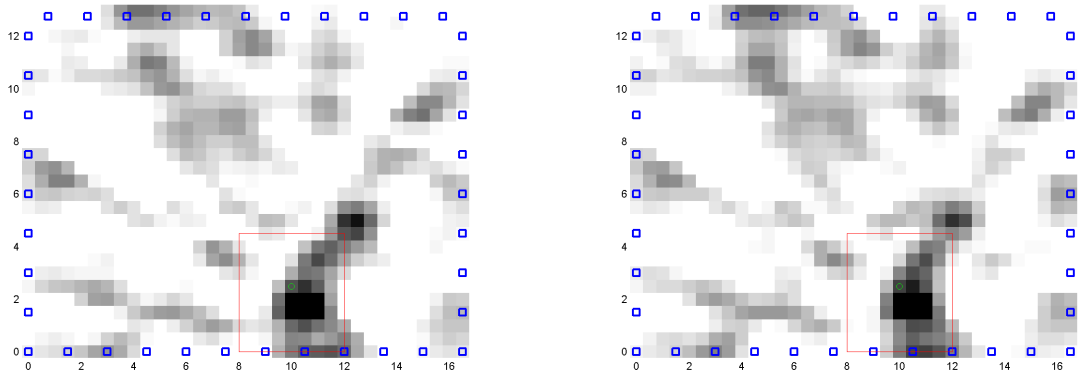

Figure 49. RTI image with Radio Map decision region for 39 motes location (10, 2.5)

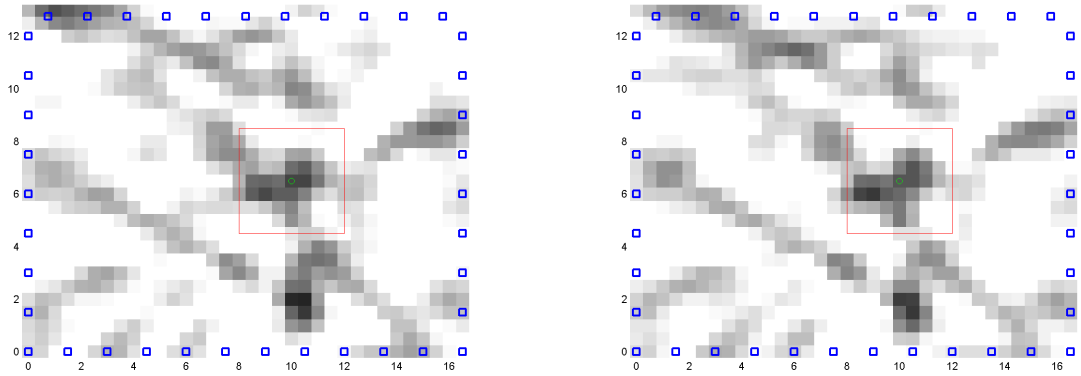

Figure 50. RTI image with Radio Map decision region for 39 motes location (10, 6.5)

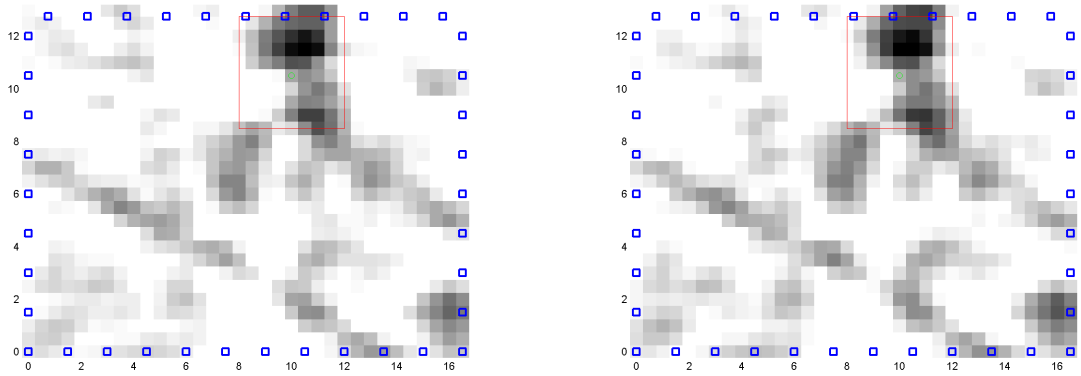

Figure 51. RTI image with Radio Map decision region for 39 motes location (10, 10.5)

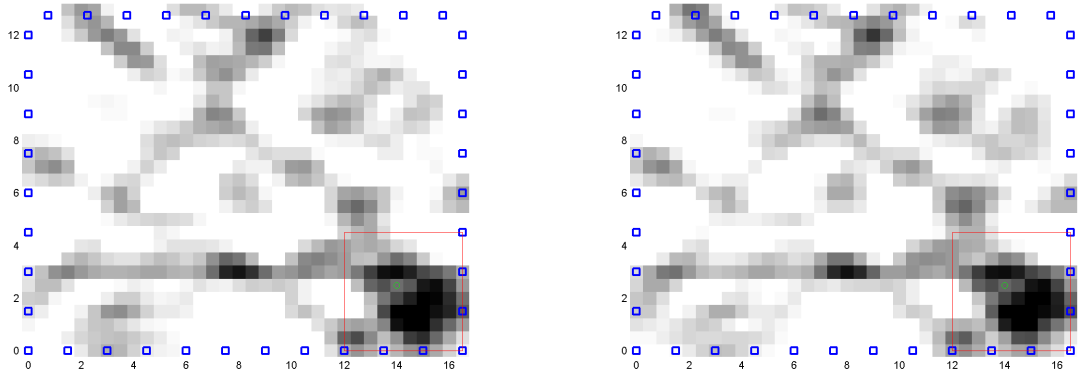

Figure 52. RTI image with Radio Map decision region for 39 motes location (14, 2.5)

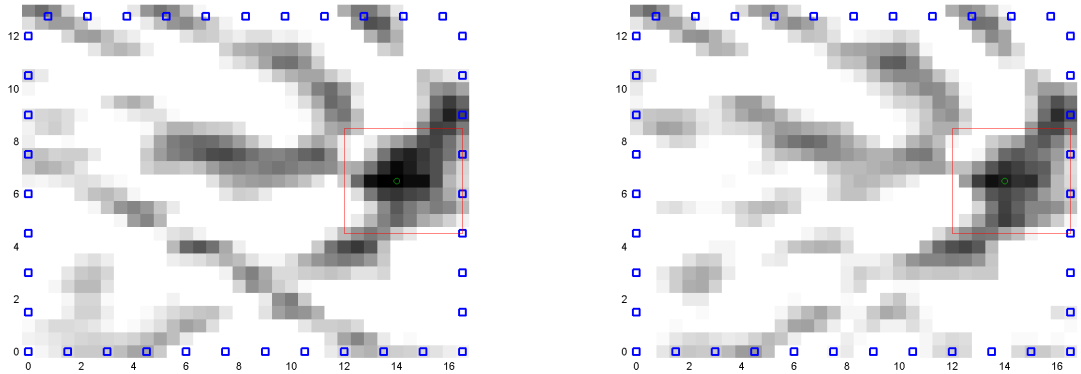

Figure 53. RTI image with Radio Map decision region for 39 motes location (14, 6.5)

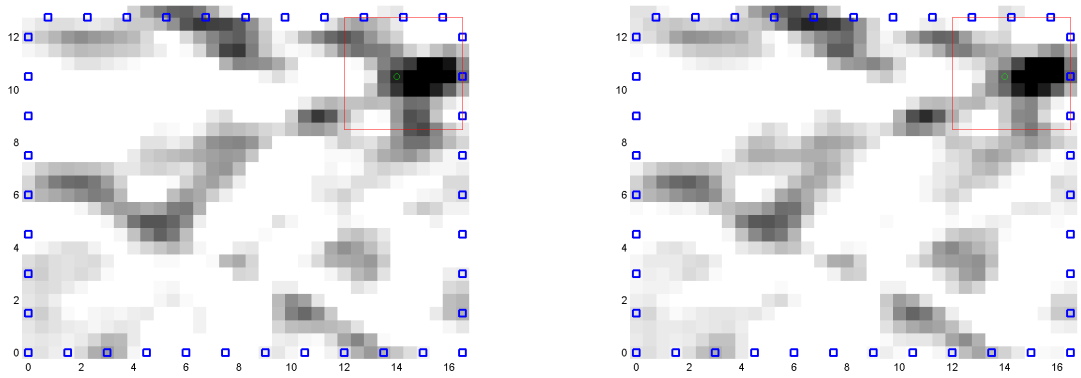

Figure 54. RTI image with Radio Map decision region for 39 motes location (14, 10.5)

C. RTI Images of 20 Mote Network

This appendix contains an additional 24 images from the 20 mote network. Out of 837 frames, 2 were chosen at random from each of the 12 calibration locations and included in the figures below. In the interest of space, the legends and axis labels have been removed, but they are identical to the figures displayed in section 4.2.

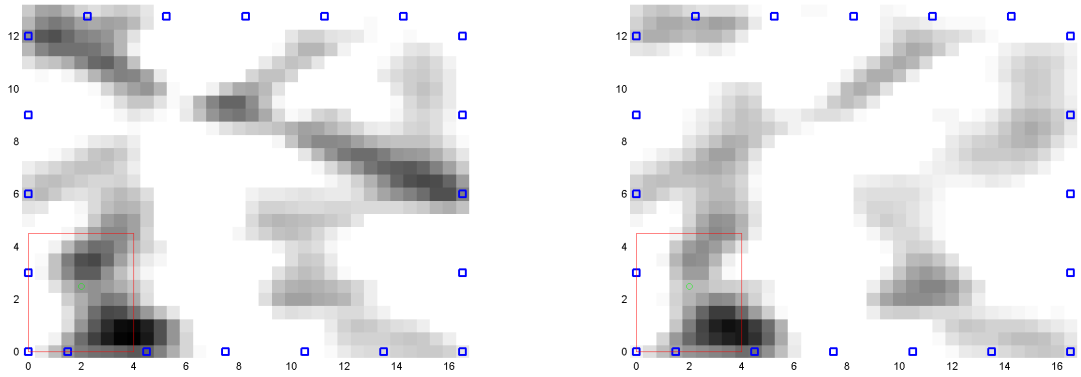

Figure 55. RTI image with Radio Map decision region for 20 motes location (2, 2.5)

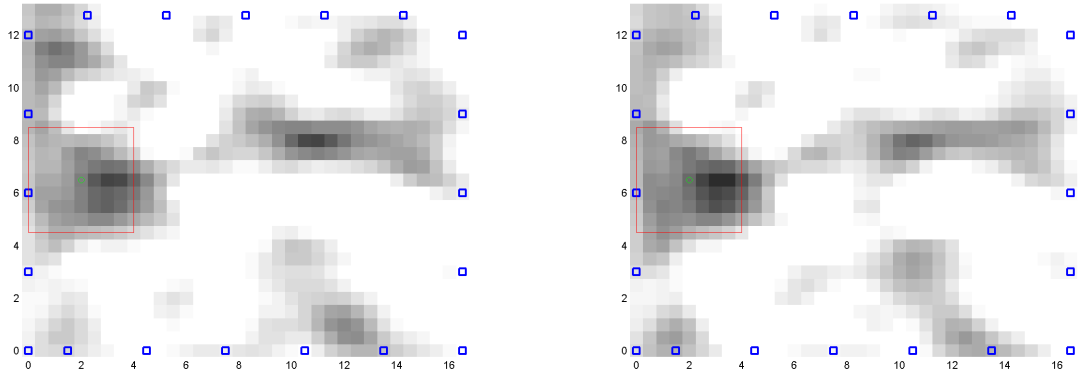

Figure 56. RTI image with Radio Map decision region for 20 motes location (2, 6.5)

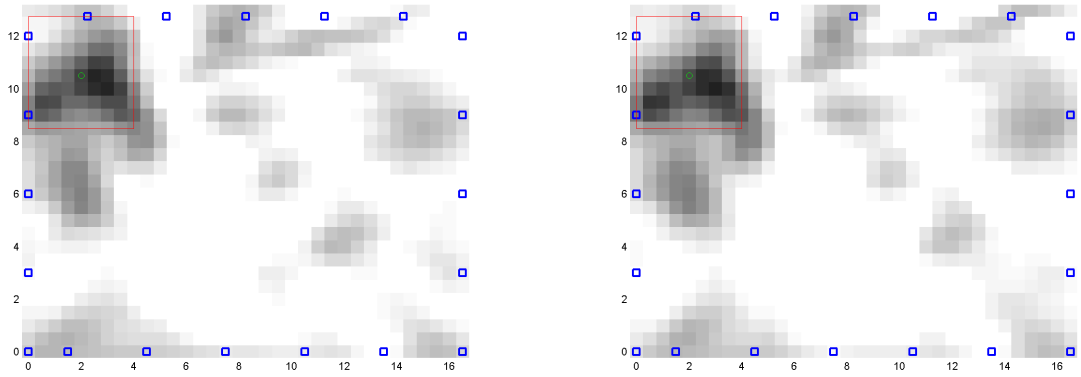

Figure 57. RTI image with Radio Map decision region for 20 motes location (2, 10.5)

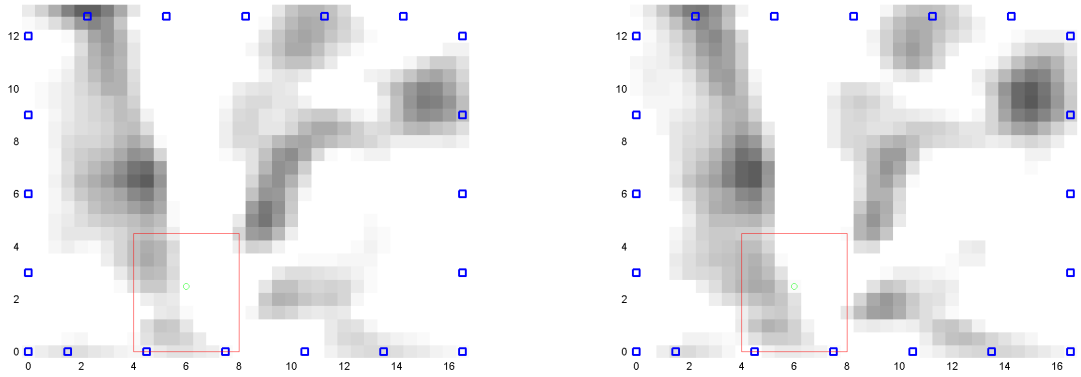

Figure 58. RTI image with Radio Map decision region for 20 motes location (6, 2.5)

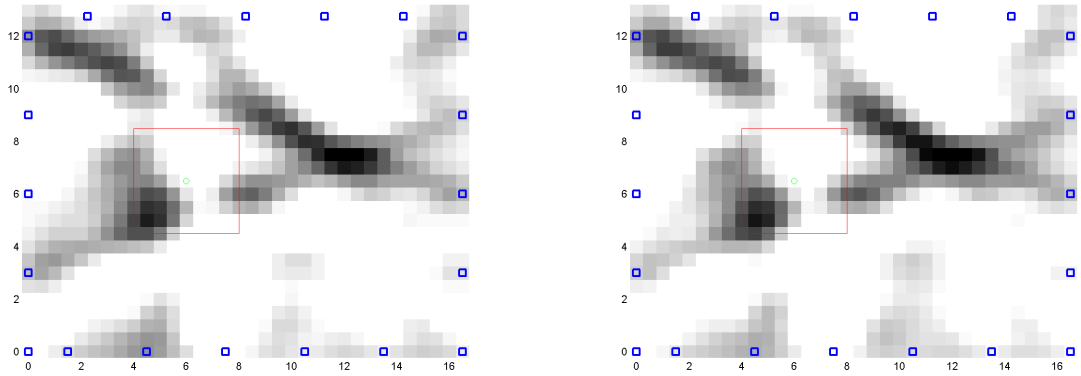

Figure 59. RTI image with Radio Map decision region for 20 motes location (6, 6.5)

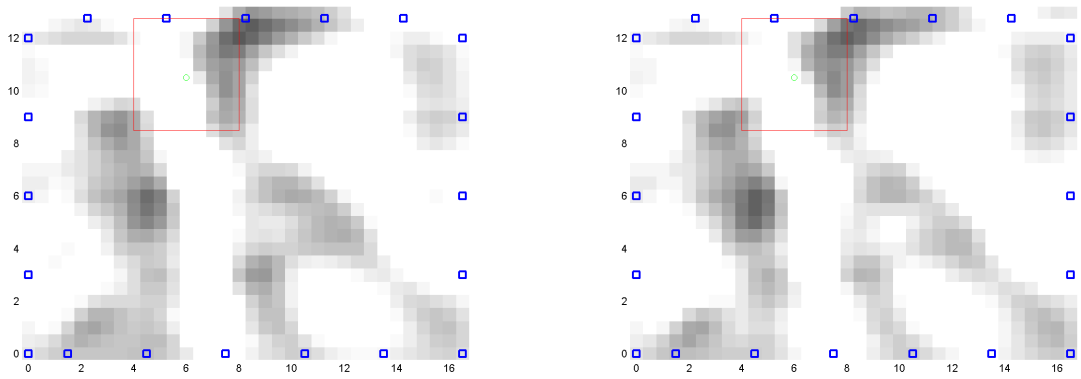

Figure 60. RTI image with Radio Map decision region for 20 motes location (6, 10.5)

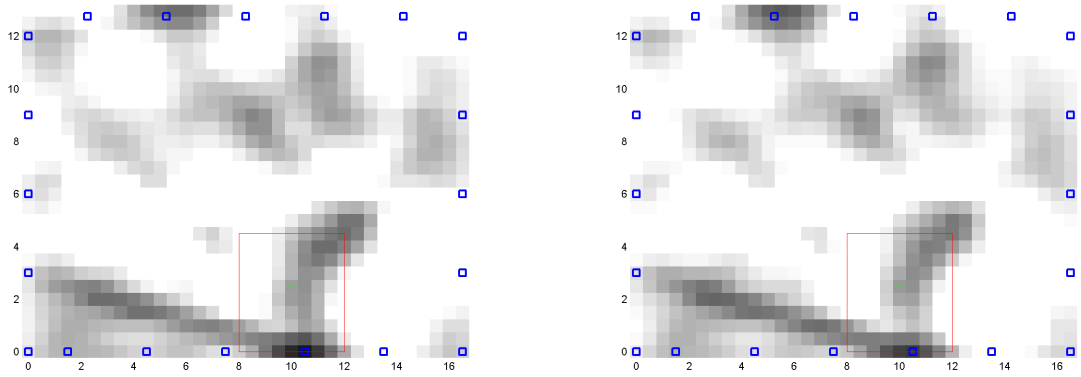

Figure 61. RTI image with Radio Map decision region for 20 motes location (10, 2.5)

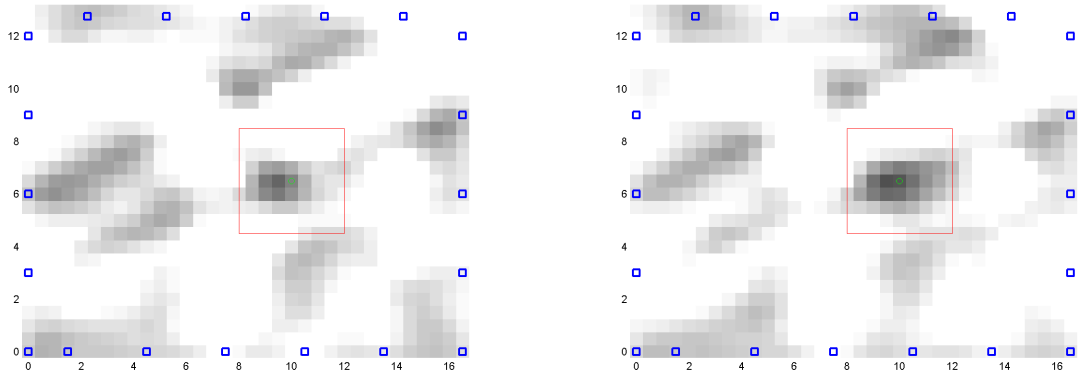

Figure 62. RTI image with Radio Map decision region for 20 motes location (10, 6.5)

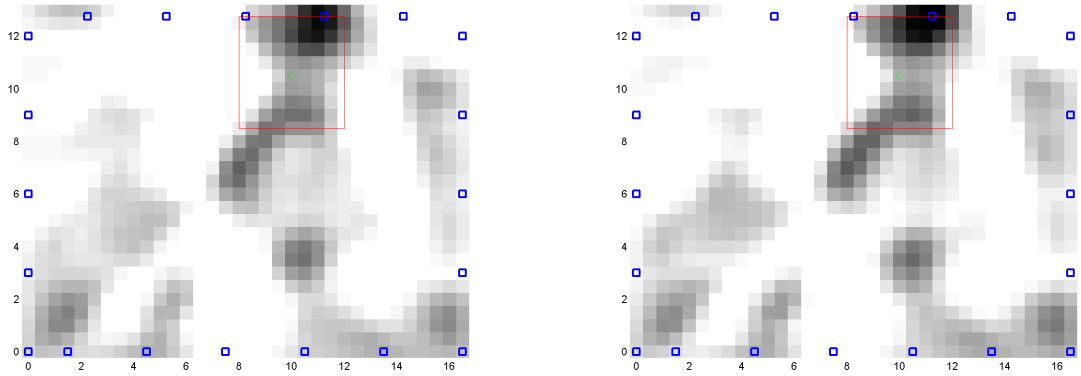

Figure 63. RTI image with Radio Map decision region for 20 motes location (10, 10.5)

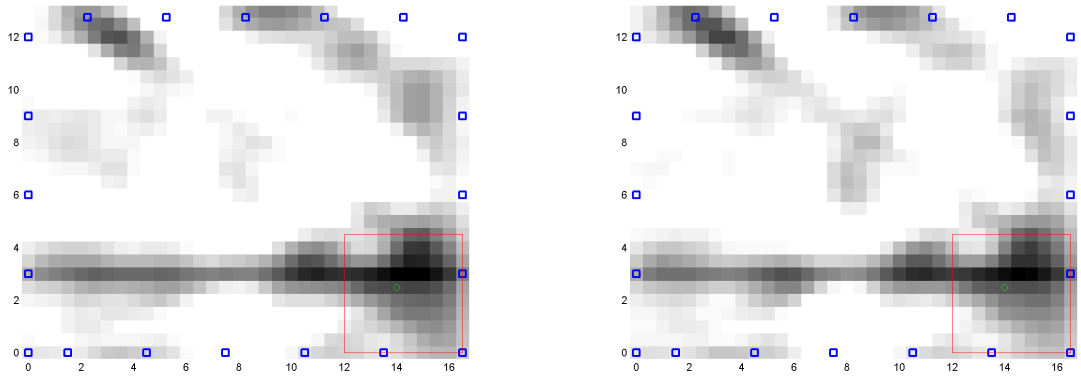

Figure 64. RTI image with Radio Map decision region for 20 motes location (14, 2.5)

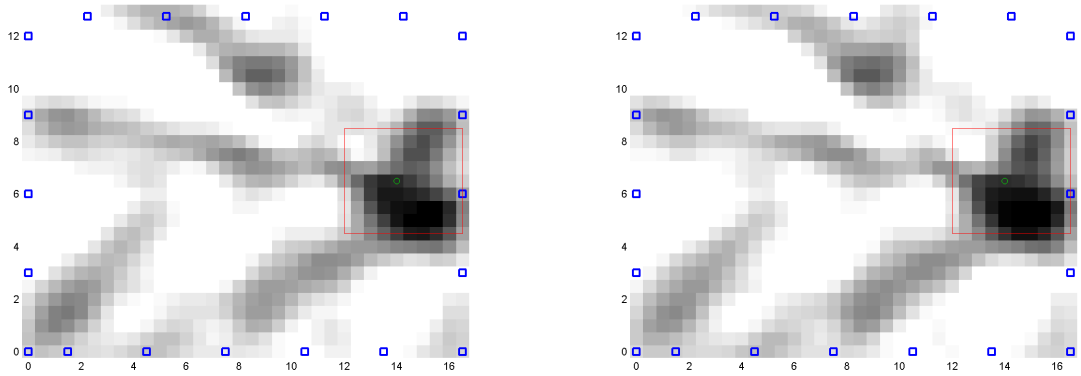

Figure 65. RTI image with Radio Map decision region for 20 motes location (14, 6.5)

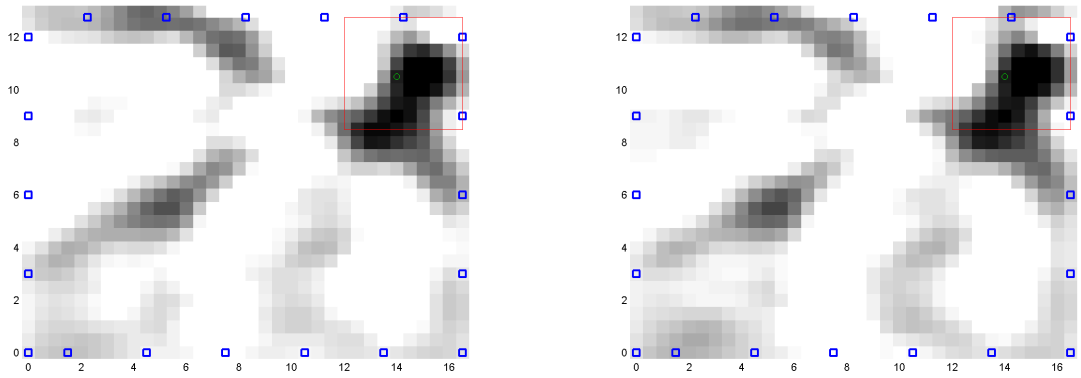

Figure 66. RTI image with Radio Map decision region for 20 motes location (14, 10.5)

Bibliography

1. J. Wilson and N. Patwari, "Radio Tomographic Imaging with Wireless Networks," *IEEE Transactions on Mobile Computing*, vol. 9, no. 5, pp. 621–632, May 2010.

2. M. Youssef, M. Mah, and A. Agrawala, "Challenges: Device-Free Passive Localization for Wireless Environments," in *Proceedings of the 13th Annual ACM International Conference on Mobile Computing and Networking*, Montreal, Quebec, Sept. 2007, pp. 222–229.

3. M. E. Brak and M. Essaaidi, "Wireless Sensor Network in Home Automation Network and Smart Grid," in *2012 International Conference on Complex Systems*, Agadir, Morocco, Nov. 2012, pp. 1–6.

4. R. K. Martin, J. Nishida, and T. Van, "Complexity Reduction in Large Scale Radio Tomography Networks," *Submitted to IEEE Transactions on Computational Imaging*, Dec. 2014.

5. D. Zhang, J. Ma, Q. Chen, and L. M. Ni, "An RF-Based System for Tracking Transceiver-Free Objects," in *Proc. Fifth Annual IEEE Int'l Conf. on Pervasive Computing and Communications (PerCom)*, Mar. 2007, pp. 135–144.

6. N. Pirzada, M. Y. Nayan, F. Subhan. M. F. Hassan, and M. A. Khan, "Device-Free Localization Technique for Indoor Detection and Tracking of Human Body: A Survery," in *Internation Conference on Innovation, Management and Technology Research*. ScienceDirect, Sep. 2013, pp. 422–429.

7. N. Patwari, J.N. Ash, S. Kyperountas, Spyros, A.O. Hero III, R.L. Moses, and N.S. Correal, "Locating the Nodes: Cooperative Localization in Wireless Sensor Networks," *Signal Processing Magazine*, vol. 22, no. 4, pp. 54–69, 2005.

8. O. Kaltiokallio, M. Bocca, and N. Patwari, "A Fade Level-Based Spatial Model for Radio Tomographic Imaging," *IEEE Transactions on Mobile Computing*, vol. PP, no. 99, pp. 1–14, 2013.

9. J. Wilson and N. Patwari, "Radio Tomographic Imaging with Wireless Networks," *Transactions on Mobile Computing*, vol. 9, no. 5, pp. 621–632, Jan. 2010.

10. R. K. Martin, A. Folkerts, and T. Heinl, "Accuracy vs. Resolution in Radio Tomography," *IEEE Transactions on Signal Processing*, vol. 62, no. 10, pp. 2480–2491, May 2014.

11. S. Nannuru, L. Yunpeng, Y. Zeng, M. Coates, and B. Yang, "Radio-Frequency Tomography for Passive Indoor Multitarget Tracking," *IEEE Transactions on Mobile Computing*, vol. 12, no. 12, pp. 2322–2333, Dec. 2013.

12. B.R. Hamilton, X. Ma, B.J. Baxley, and S.M. Matechik, "Propagation Modeling for Radio Frequency Tomography in Wireless Networks," *Journal of Selected Topics in Signal Processing: Special Issue on Non-Cooperative Localization Networks*, vol. 8, no. 1, Oct. 2013.

13. O. Kaltiokallio, M. Bocca, and N. Patwari, "Enhancing the Accuracy of Radio Tomographic Imaging Using Channel Diversity," in *IEEE 9th International Conference on Mobile Adhoc and Sensor Systems (MASS)*, Oct. 2012, pp. 254–262.

14. J. Wilson, N. Patwari, and F.G. Vasquez, "Regularization Methods for Radio Tomographic Imaging," in *Proc. Virginia Tech Symposium on Wireless Personal Communications*, Jun. 2009.

15. L. Heng, W. Zheng-huan, B. Xiang-yuan, and A. Jian-ping, "Image Reconstruction Algorithms for Radio Tomographic Imaging," in *2012 IEEE International Conference on Cyber Technology in Automation, Control, and Intelligent Systems*, Bangkok, Thailand, May 2012, pp. 48–53.

16. C. R. Anderson, R. K. Martin, T. O. Walker, and R. W. Thomas, "Radio Tomography for Roadside Surveillance," *IEEE Journal of Selected Topics in Signal Processing: Special Issue on Non-Cooperative Localization Networks*, vol. 8, no. 1, Feb. 2014.

17. Y. Mostofi and A. Gonzalez-Ruiz, "Compressive Cooperative Obstacle Mapping in Mobile Networks," in *Proc. Conf. on Military Communications (MILCOM)*. IEEE, 2010, pp. 524–530.

18. M. A. Kanso and M. G. Rabbat, "Compressed RF Tomography for Wireless Sensor Networks: Centralized and Decentralized Approaches," in *IEEE Proc. Fifth Int'l Conf. on Distributed Computing in Sensor Systems (DCOSS)*, pp. 173–186. Springer, 2009.

19. R. K. Martin, C. Anderson, R. W. Thomas, and A. S. King, "Modelling and Analysis of Radio Tomography," in *2011 Fourth IEEE Int'l Workshop on Computational Advances in Multi-Sensor Adaptive Processing (CAMSAP)*, San Juan, Puerto Rico, Dec. 2011, pp. 377–380.

20. N. Patwari and P. Agrawal, "Effects of Correlated Shadowing: Connectivity, Localization, and RF Tomography," in *Proc. Int'l Conf. on Information Processing in Sensor Networks (IPSN)*. IEEE, 2008, pp. 82–93.

21. Y. Zhao and N. Patwari, "Noise Reduction for Variance-Based Device-Free Localization and Tracking," in *Proc. Eighth Conf. on Sensor, Mesh and Ad Hoc Communications and Networks (SECON)*. IEEE, 2011, pp. 179–187.

22. O. Kaltiokallio, M. Bocca, and N. Patwari, "Enhancing the Accuracy of Radio Tomographic Imaging using Channel Diversity," in *Proc. IEEE Ninth Int'l Conf. on Mobile Adhoc and Sensor Systems (MASS)*, Oct. 2012, pp. 254–262.

23. J. Wilson and N. Patwari, "See-Through Walls: Motion Tracking using Variance-Based Radio Tomography Networks," *IEEE Transactions on Mobile Computing*, vol. 10, no. 5, pp. 612–621, Sep. 2011.

24. J. Wilson and N. Patwari, "A Fade-Level Skew-Laplace Signal Strength Model for Device-Free Localization with Wireless Networks," *IEEE Transactions on Mobile Computing*, vol. 11, no. 6, pp. 947–958, 2012.

25. J. Wilson and N. Patwari, "Through-Wall Tracking Using Variance-Based Radio Tomography Networks," *arXiv preprint arXiv:0909.5417*, Sep. 2009.

26. Y. Zhao, N. Patwari, J. M. Phillips, and S. Venkatasubramanian, "Radio Tomographic Imaging and Tracking of Stationary and Moving People via Kernel Distance," in *2013 ACM/IEEE International Conference on Information Processing in Sensor Networks (IPSN)*, Apr. 2013, pp. 229–240.

27. M. Moussa and M. Youssef, "Smart devices for smart environments: Device-free passive detection in real environments," in *Pervasive Computing and Communications, 2009. PerCom 2009. IEEE International Conference on*, March 2009, pp. 1–6.

28. Mu Zhou, Qiao Zhang, Zengshan Tian, Feng Qiu, and Qi Wu, "Correlated received signal strength correction for radio-map based indoor wi-fi localization," in *Computing, Communication and Networking Technologies (ICCCNT), 2014 International Conference on*, July 2014, pp. 1–6.

29. Xiongfei Geng, Yongcai Wang, Haoran Feng, and Zhoufeng Chen, "Hybrid radio-map for noise tolerant wireless indoor localization," in *Networking, Sensing and Control (ICNSC), 2014 IEEE 11th International Conference on*, April 2014, pp. 233–238.

30. P.M. Scholl, S. Kohlbrecher, V. Sachidananda, and K. Van Laerhoven, "Fast indoor radio-map building for rssi-based localization systems," in *Networked Sensing Systems (INSS), 2012 Ninth International Conference on*, June 2012, pp. 1–2.

31. Hui Wang, "Bayesian radio map learning for robust indoor positioning," in *Indoor Positioning and Indoor Navigation (IPIN), 2011 International Conference on*, Sept 2011, pp. 1–6.

32. Crossbow Technologies, "TelosB Mote Platform Datasheet," Webpage, `https://www.willow.co.uk/TelosB_Datasheet.pdf`, 2013.

33. Stanford Research Community, "TinyOS Home Page," Webpage, `http://www.tinyos.net`, 2007-2013.

REPORT DOCUMENTATION PAGE

Form Approved
OMB No. 0704–0188

1. REPORT DATE *(DD–MM–YYYY)*	2. REPORT TYPE	3. DATES COVERED *(From — To)*
24-03-2016	Master's Thesis	SEP 2014 - MAR 2016

4. TITLE AND SUBTITLE

Comparison of Methods for Radio Position of Non-Emitting Dismounts

5a. CONTRACT NUMBER

5b. GRANT NUMBER

5c. PROGRAM ELEMENT NUMBER

6. AUTHOR(S)

Seanor, Collin J Captain, USAF

5d. PROJECT NUMBER

5e. TASK NUMBER

5f. WORK UNIT NUMBER

7. PERFORMING ORGANIZATION NAME(S) AND ADDRESS(ES)

Air Force Institute of Technology
Graduate School of Engineering and Management (AFIT/EN)
2950 Hobson Way
WPAFB OH 45433-7765

8. PERFORMING ORGANIZATION REPORT NUMBER

AFIT-ENG-MS-16-M-044

9. SPONSORING / MONITORING AGENCY NAME(S) AND ADDRESS(ES)

Intentionally Left Blank

10. SPONSOR/MONITOR'S ACRONYM(S)

11. SPONSOR/MONITOR'S REPORT NUMBER(S)

12. DISTRIBUTION / AVAILABILITY STATEMENT

DISTRIBUTION STATEMENT A:
APPROVED FOR PUBLIC RELEASE; DISTRIBUTION UNLIMITED.

13. SUPPLEMENTARY NOTES

14. ABSTRACT

RTI is a form of DFPL that utilizes the RSS values from a collection of wireless transceivers to produce an image in order to localize a subject within a WSN. Radio Mapping is another form of DFPL that can utilize the same RSS values from a WSN to localize a subject by comparing recent values to a set of calibration data. RTI and Radio Mapping have never been directly compared to one another as a means of localization within a WSN. The goal of this research is to compare these approaches in a side by side manner. A real world WSN was constructed and both RTI and Radio Mapping methodologies were applied to identical data sets with the results compared and discussed. Initial results show that both methodologies have inherent advantages and disadvantages respective to one another; Radio Mapping performs significantly better in WSNs with a low number of transceivers, while RTI has significantly more simple calibration procedures.

15. SUBJECT TERMS

Radio Tomographic Imaging, Radio Map, Wireless Sensor Network, Received Signal Strength

16. SECURITY CLASSIFICATION OF:			17. LIMITATION OF ABSTRACT	18. NUMBER OF PAGES	19a. NAME OF RESPONSIBLE PERSON
a. REPORT	b. ABSTRACT	c. THIS PAGE			Dr. Richard K Martin, AFIT/ENG
U	U	U	U	88	19b. TELEPHONE NUMBER *(include area code)* (937) 785-3636, x4625; Richard.Martin@afit.edu